J. Fluid Mech. (1989), *vol.* 206, *pp.* 433–462
Printed in Great Britain

Wave–vortex dynamics in rotating shallow water

By MARIE FARGE AND ROBERT SADOURNY
Laboratoire de Météorologie Dynamique du CNRS, 24, rue Lhomond,
75231 Paris Cedex 05, France

(Received 24 November 1987 and in revised form 28 March 1989)

We investigate how two-dimensional turbulence is modified when the incompressibility constraint is removed, by numerically integrating the full Saint-Venant (shallow-water) equations. In the case of small geopotential fluctuations considered here, we find no energy exchange between the inertio–gravitational and the potentio–vortical components of the flow. At small scales, the potentio–vortical component behaves as if the flow were incompressible, while we observe an intense direct energy cascade within the inertio–gravitational component. At large scales, the reverse potentio–vortical energy cascade is reduced when the level of inertio–gravitational energy is high. Looking at the effect of rotation, we find that a fast rotation rate tends to inhibit all three cascades. In particular, the inhibition of the inertio–gravitational energy cascade towards small scales implies that the geostrophic adjustment process is hindered by an increase of rotation. Concerning the structure of the coherent vortices emerging out of these decaying turbulent flows, we observe that the smallest scales are concentrated inside the vortex cores and not on their periphery.

1. Introduction

Two-dimensional turbulence has been intensively studied in the last 20 years. Initially considered as a somewhat academic topic, it has gradually evolved from theory, based on dimensional analysis (Kraichnan 1967; Leith 1968; Batchelor 1969), to verifiable modelling of real flows, observed in the atmosphere and ocean (Morel & Larchevêque 1974; Desbois 1975; Boer & Shepherd 1983), or produced in the laboratory (Hopfinger 1983; Sommeria 1986; Couder 1984). In fact, the development of numerical simulation using vector computers has allowed a detailed exploration, realistic and systematic, that self-similarity theory alone, even supported by more sophisticated models of statistical closure, could not offer (Basdevant *et al.* 1981; Babiano *et al.* 1984; McWilliams 1984). A more general concept, better suited to stratified geophysical fluids, was also developed and studied under the topic of baroclinic quasi-geostrophic turbulence (Charney 1971; Rhines 1979; Salmon 1978; Hoyer & Sadourny 1982; Sadourny 1985).

These theories and models have proved their relevance to the description of the dynamics of large-scale atmospheric or oceanographic flows far from the equator, i.e. under conditions where the quasi-geostrophic hypothesis (weak horizontal divergence and dominance of rotational eddies over inertio–gravitational waves) is actually verified. However, we may emphasize that the mechanisms generating quasi-geostrophy are not always clearly understood, even in the simple barotropic case of shallow-water equations. In the theories of Cahn (1945) and Obukhov (1949), it is the dispersion of inertio–gravity waves over an infinite domain which allows the

potentio–vortical modes, left behind, to dominate; but this linear argument, reasonable for a flow having initially a limited extension on the infinite plane, does not apply for a finite or periodic domain like the sphere. Sadourny (1975) has proposed a nonlinear mechanism, where inertio–gravitational energy would be removed by cascading towards small scales, giving way to the prevalence of rotational eddies which, instead, remain trapped within the larger scales.

The trend towards a quasi-geostrophic attractor of solutions of the Saint-Venant equations driven by constant forcing and dissipation (Lorenz 1980) is also a clear indication of the nonlinearity of the geostrophic adjustment process. The central problem of nonlinear interactions between geostrophic (or potentio–vortical) modes and ageostrophic (or inertio–gravitational) modes has been addressed by Sadourny (1975) and Warn (1986) for the Saint-Venant equations, while Errico (1981, 1984) has investigated similar questions for a two-layer model. Our purpose here is to study the nonlinear behaviour of inertio–gravitational waves and their influence on the geostrophic dynamics, under various magnitudes of the rotation rate.

2. Basic formulations and definitions

We consider shallow-water motion of mean depth H over a doubly periodic plane rotating with uniform angular velocity Ω. Taking the Coriolis parameter $f^{-1} = (2\Omega)^{-1}$ as unit time and the radius of deformation $(gH)^{\frac{1}{2}}/f$ as unit length, g being the acceleration due to gravity, we write the adimensional form of the Saint-Venant (shallow-water) equations as

$$\left.\begin{aligned} &\frac{\partial \boldsymbol{V}}{\partial t} + (1 + \boldsymbol{N}\cdot(\boldsymbol{\nabla}\times\boldsymbol{V}))\,\boldsymbol{N}\times\boldsymbol{V} + \boldsymbol{\nabla}(\phi + \tfrac{1}{2}V^2) = 0, \\ &\frac{\partial \phi}{\partial t} + \boldsymbol{\nabla}\cdot\{(1+\phi)\,\boldsymbol{V}\} = 0, \end{aligned}\right\} \tag{1}$$

in the absence of sources and dissipation. In (1) $\boldsymbol{N}$ refers to the vertical unit vector oriented upwards, $\boldsymbol{V}$ to the horizontal velocity measured with the unit $(gH)^{\frac{1}{2}}$, and ϕ to the relative fluctuations of the free-surface geopotential around its mean value of unity. Shallow-water flow can be termed 'divergent', or 'compressible two-dimensional', because the surface height acts as a variable two-dimensional density producing divergent motions and a combination of inertial and gravity waves. It has a formal analogy with barotropic three-dimensional compressible flow under the condition $\gamma = c_p/c_v = 2$ (Riabouchinsky 1932). Following this formal analogy, we shall hereafter call $\langle|\boldsymbol{V}|\rangle/(gH)^{\frac{1}{2}}$ (where the angle brackets means averaged on the plane) the Mach number of the shallow-water flow. Its dynamics is then sensitive to a constant Coriolis force for scales larger than the Rossby deformation radius, which is not the case for non-divergent two-dimensional flows. In the absence of dissipation, total energy, defined as the sum of potential plus kinetic energy,

$$E = \frac{1}{2}\iint \{\phi^2 + (1+\phi)\,V^2\}\,\mathrm{d}x\,\mathrm{d}y, \tag{2}$$

is an integral invariant of the motion. Also in the absence of dissipation, potential vorticity, defined as

$$q = (1 + \boldsymbol{N}\cdot(\boldsymbol{\nabla}\times\boldsymbol{V}))/(1+\phi), \tag{3}$$

is a Lagrangian invariant, associated with an infinite number of integral invariants, amongst which is potential enstrophy

$$S = \frac{1}{2}\iint q^2(1+\phi)\,\mathrm{d}x\,\mathrm{d}y. \tag{4}$$

The linearized equations for small perturbations around a resting state with free-surface height H are readily obtained from (1):

$$\frac{\partial \boldsymbol{V}}{\partial t} + \boldsymbol{N}\cdot(\boldsymbol{\nabla}\times\boldsymbol{V}) + \boldsymbol{\nabla}\phi = 0, \quad \frac{\partial \phi}{\partial t} + \boldsymbol{\nabla}\cdot\boldsymbol{V} = 0, \tag{5}$$

or, in terms of stream function $\psi = \nabla^{-2}(\boldsymbol{N}\cdot(\boldsymbol{\nabla}\times\boldsymbol{V}))$ and velocity potential $\chi = \nabla^{-2}(\boldsymbol{\nabla}\cdot\boldsymbol{V})$:

$$\frac{\partial \psi}{\partial t} + \chi = 0, \quad \frac{\partial \chi}{\partial t} - \psi + \phi = 0, \quad \frac{\partial \phi}{\partial t} + \nabla^2\chi = 0. \tag{6}$$

These linearized equations (5), (6) have quadratic invariants corresponding to the non-quadratic invariants, energy (2) and potential enstrophy (4), of the nonlinear case (1). The perturbation energy is

$$E' = \frac{1}{2}\iint (\phi^2 + V^2)\,\mathrm{d}x\,\mathrm{d}y, \tag{7}$$

and the perturbation potential enstrophy is

$$S' = \frac{1}{2}\iint q'^2\,\mathrm{d}x\,\mathrm{d}y, \tag{8}$$

with

$$q' = \boldsymbol{N}\cdot(\boldsymbol{\nabla}\times\boldsymbol{V}) - \phi = \nabla^2\psi - \phi \tag{9}$$

being the linearized potential vorticity of the perturbation. Owing to the existence of the quadratic invariant E', equations (5), (6) have a complete set of eigenmodes, clearly divided into two classes: (i) the potentio–vortical mode (denoted by the subscript V), which is non-divergent ($\chi_{\mathrm{V}} = 0$), geostrophic ($\phi_{\mathrm{V}} = \psi_{\mathrm{V}}$), stationary (the associated eigenfrequencies vanish, $\omega_{\mathrm{V}} = 0$) and which contains all the linearized potential vorticity of the flow ($q'_{\mathrm{V}} = q'$); (ii) the two inertio–gravitational modes (denoted by the subscript G) also called Poincaré waves, which are divergent ($\chi_{\mathrm{G}} = \chi$), characterized by their high frequencies ($\omega_{\mathrm{G}}^2 = 1 + k^2$, k being the magnitude of the wavevector) and for which the linearized potential vorticity vanishes ($q'_{\mathrm{G}} = 0$ or $k^2\psi_{\mathrm{G}} = -\phi_{\mathrm{G}}$). In the limit of no rotation these inertio–gravity modes propagate with the critical velocity $(gH)^{\frac{1}{2}}$ (= 1 in our adimensional formulation). This critical velocity is the equivalent of the sound velocity for our problem, following the analogy already stated with three-dimensional barotropic flow (Riabouchinsky 1932). In the presence of rotation, inertio–gravity modes become dispersive.

This decomposition into orthogonal eigenmodes is analogous, in the limit $f \to 0$, to the factorization used to describe compressible (Moyal 1952; Feiereisen, Reynolds & Ferziger 1981) or axisymmetric (Craya 1958; Herring 1974) turbulence, where the velocity field in Fourier space is decomposed into a solenoidal (dilatation-free) vector and a dilatation vector, respectively perpendicular and parallel to the wave vector. An equivalent decomposition into potential vorticity and internal wave modes has been proposed to analyse stratified flows (Riley, Metcalfe & Weissman 1981; Lilly 1983; Müller, Lien & Williams 1988). Note that the slow-manifold characteristic of

balanced states, introduced by Leith (1980) and Lorenz (1980, 1986), is an extension to the nonlinear case of the subspace of potentio–vortical modes.

Energy (2) and potential enstrophy (4) are strict invariants of the nonlinear equations (1); but, being non-quadratic, they cannot be split unequivocally into the various scales, as is usually done in the incompressible† case using Fourier series. On the other hand, spectral expansions can be computed using the eigenmodes of the linearized equations, from which spectral distributions of E' and S' can be obtained; but E' and S' are approximate invariants of the nonlinear equations only in the small-perturbation quasi-incompressible limit. On the basis of these eigenmodes, we define a one-dimensional potentio–vortical energy spectrum

$$E'_{\mathrm{V}}(k_n) = \frac{1}{2} \sum_{k_n \leqslant |k| < k_{n+1}} \frac{|k^2\psi(\boldsymbol{k}) + \phi(\boldsymbol{k})|^2}{1+k^2}, \tag{10}$$

and a one-dimensional inertio–gravitational energy spectrum

$$E'_{\mathrm{G}}(k_n) = \frac{1}{2} \sum_{k_n \leqslant |k| < k_{n+1}} k^2 \left\{ \frac{|\chi(\boldsymbol{k})|^2 + |\psi(\boldsymbol{k}) - \phi(\boldsymbol{k})|^2}{1+k^2} \right\}, \tag{11}$$

which appears as the sum of divergent energy plus ageostrophic energy. The corresponding potential enstrophy spectra read

$$S'_{\mathrm{V}}(k_n) = \frac{1}{2} \sum_{k_n \leqslant |k| < k_{n+1}} |k^2\psi(\boldsymbol{k}) + \phi(\boldsymbol{k})|^2, \tag{12}$$

$$S'_{\mathrm{G}}(k_n) = 0. \tag{13}$$

The global linearized invariants, expressed as

$$\left.\begin{aligned} E' &= \sum_n \{E'_{\mathrm{V}}(k_n) + E'_{\mathrm{G}}(k_n)\}, \\ S' &= \sum_n \{S'_{\mathrm{V}}(k_n) + S'_{\mathrm{G}}(k_n)\}, \end{aligned}\right\} \tag{14}$$

are, to first order, equivalent to E and S in the weak perturbation limit.

Note that the quadratic forms E' and S' are, in fact, exact invariants of the nonlinear system

$$\left.\begin{aligned} &\frac{\partial}{\partial t}\nabla^2\psi + J(\psi, \nabla^2\psi) + \nabla^2\chi = 0, \\ &\frac{\partial}{\partial t}\nabla^2\chi + J(\chi, \nabla^2\psi) + \nabla^2(\phi - \psi) = 0, \\ &\frac{\partial\phi}{\partial t} + J(\psi, \phi) + \nabla^2\chi = 0, \end{aligned}\right\} \tag{15}$$

which is intermediate between (1) and (5); it is obtained by rewriting (1) in terms of ψ, χ and ϕ, then dropping all nonlinear terms that are not in Jacobian form. A variant of (15), which also exactly conserves E' and S', can be obtained by dropping

† In the present context the word 'incompressible' means that the two-dimensional density (or free-surface height) of a fluid parcel is conserved within the two-dimensional fluid motion. The classical theory of two-dimensional turbulence deals with incompressible two-dimensional flow, in this sense.

$J(\chi, \nabla^2\psi)$ in the divergence equation, which reduces then to its linear part. From (15), or its variant, we get

$$\frac{\partial}{\partial t}(\nabla^2\psi - \phi) + J(\psi, \nabla^2\psi - \phi) = 0, \tag{16}$$

which, in the quasi-geostrophic case ($\phi - \psi = 0$), yields the barotropic non-divergent potential vorticity equation

$$\frac{\partial}{\partial t}(\nabla^2 - 1)\,\psi + J(\psi, \nabla^2\psi) = 0. \tag{17}$$

Thus (15), or its variant, also appears as an intermediate form between the full Saint-Venant equations and their quasi-geostrophic approximation (17).

In the quasi-geostrophic case, the one-dimensional distribution of total energy reads

$$E''(k_n) = \frac{1}{2} \sum_{k_n \leqslant |k| < k_{n+1}} (1+k^2)\,|\psi(\boldsymbol{k})|^2 = \sum_{k_n \leqslant |k| < k_{n+1}} \mathscr{E}''(\boldsymbol{k}). \tag{18}$$

The one-dimensional distributions of potential enstrophy S'', kinetic energy K'' and kinetic enstrophy Z'' are entirely determined by the modal distribution of total energy $\mathscr{E}''(\boldsymbol{k})$:

$$S''(k_n) = \sum_{k_n \leqslant |k| < k_{n+1}} (1+k^2)\,\mathscr{E}''(\boldsymbol{k}), \tag{19}$$

$$K''(k_n) = \sum_{k_n \leqslant |k| < k_{n+1}} \frac{k^2}{1+k^2}\mathscr{E}''(\boldsymbol{k}), \tag{20}$$

$$Z''(k_n) = \sum_{k_n \leqslant |k| < k_{n+1}} \frac{k^4}{1+k^2}\mathscr{E}''(\boldsymbol{k}). \tag{21}$$

Note that relation (19) is also valid for the potentio–vortical modes of the full Saint-Venant equations:

$$S'_{\mathrm{V}}(k_n) = \sum_{k_n \leqslant |k| < k_{n+1}} (1+k^2)\,\mathscr{E}'_{\mathrm{V}}(\boldsymbol{k}) \tag{22}$$

with $$\mathscr{E}'_{\mathrm{V}}(\boldsymbol{k}) = \frac{|k\psi(\boldsymbol{k}) + \phi(\boldsymbol{k})|^2}{1+k^2}.$$

3. The quasi-geostrophic case

We first look at the effect of rotation on quasi-geostrophic dynamics. The basic spectral relations are (18)–(21); the classical relations of two-dimensional turbulence are recovered when $k \gg 1$ (scales smaller than the radius of deformation); the spectral range $k < 1$ corresponds to the range of scales where the flow is sensitive to rotation. For simplicity we consider the case of a stationary turbulent flow in an infinite rotating plane, forced at $k = k_I$ and dissipated at $k = k_D \gg k_I$. We denote by I_E, I_S the energy and potential enstrophy injection rates, and by D_E, D_S the corresponding dissipation rates. From (19),

$$I_S = (1+k_I^2)\,I_E, \quad D_S = (1+k_D^2)\,D_E. \tag{23}$$

For stationary turbulence we have $D_S \leqslant I_S$ and therefore, $D_E \to 0$ as $k_D \to \infty$: as in usual two-dimensional turbulence, energy is not dissipated at infinite Reynolds

numbers. Denoting now by L_E, L_S the rates of total energy and potential enstrophy reaching a given large scale range $k \leqslant k_L \ll k_I$, we get, again from (19),

$$L_E < L_S \leqslant (1+k_L^2) L_E. \tag{24}$$

Stationarity in the range $k_L < k < k_D$ implies $I_E = L_E + D_E$, $I_S = L_S + D_S$, hence in the limit $k_D \to \infty$, $k_L \to 0$,

$$L_S = L_E = I_E, \quad D_E = 0, \quad D_S = k_I^2 I_E. \tag{25}$$

For low rotation rates (low in the sense $k_I > 1$), almost all the potential enstrophy injected is dissipated at small scales, and the same is true of kinetic enstrophy: we are almost in the classical case of incompressible two-dimensional turbulence. For high rotation rates ($k_I < 1$), potential enstrophy dissipation becomes inefficient, most of the potential enstrophy injected follows the energy in its reverse cascade towards the larger scales. For intermediate rotation rates ($k_I = 1$), half of the potential enstrophy cascades to small scales, half of it cascades to large scales. In all cases, all the energy injected goes to the largest scales available.

The characteristic time of nonlinear transfers at scale k^{-1} can be evaluated as usual from a root-mean-square measure of velocity shears at scales larger than k^{-1}, readily expressed in spectral space from the kinetic enstrophy integral:

$$\tau''(k) \sim \left\{ \int_0^k \frac{p^4}{1+p^2} E''(p)\, \mathrm{d}p \right\}^{-\frac{1}{2}}. \tag{26}$$

In the stationary regime, the energy inertial range is characterized by a constant inverse energy cascade rate $\epsilon = L_E = I_E$, which can be estimated as

$$\epsilon \sim k E''(k)/\tau''(k). \tag{27}$$

The conjunction of (26) and (27) yields a differential equation which can be integrated to determine $E''(k)$ in the range $k < k_I$:

$$E''(k) \sim \epsilon^{\frac{2}{3}} k^{-1} [k^2 - \ln(1+k^2)]^{-\frac{1}{3}}. \tag{28}$$

On the other hand, the potential enstrophy inertial range is characterized by a constant direct potential enstrophy cascade rate $\eta = D_S = k_I^2 \epsilon$, again estimated as

$$\eta \sim k S''(k)/\tau''(k). \tag{29}$$

The combination of (19), (26) and (29) yields a differential equation whose integration determines $E''(k)$ in the range $k > k_I$:

$$E''(k) \sim \eta^{\frac{2}{3}} k^{-1} (1+k^2)^{-1} \left[\ln(1+k^2) - \frac{k^2}{1+k^2} \right]^{-\frac{1}{3}}. \tag{30}$$

In the limit $k \gg 1$, i.e. at scales not affected by rotation, (28) and (30) yield the well-known spectral forms of the two-dimensional classical energy and enstrophy inertial ranges:

$$\left.\begin{aligned} E''(k) &\sim \epsilon^{\frac{2}{3}} k^{-\frac{5}{3}} && (k < k_I) \\ E''(k) &\sim \eta^{\frac{2}{3}} k^{-3} (\ln k)^{-\frac{1}{3}} && (k > k_I) \end{aligned}\right\}. \tag{31}$$

These laws hold for weak rotation ($k_I \gg 1$) in the range $k > 1$.

On the other hand, at scales larger than the radius of deformation, rotation

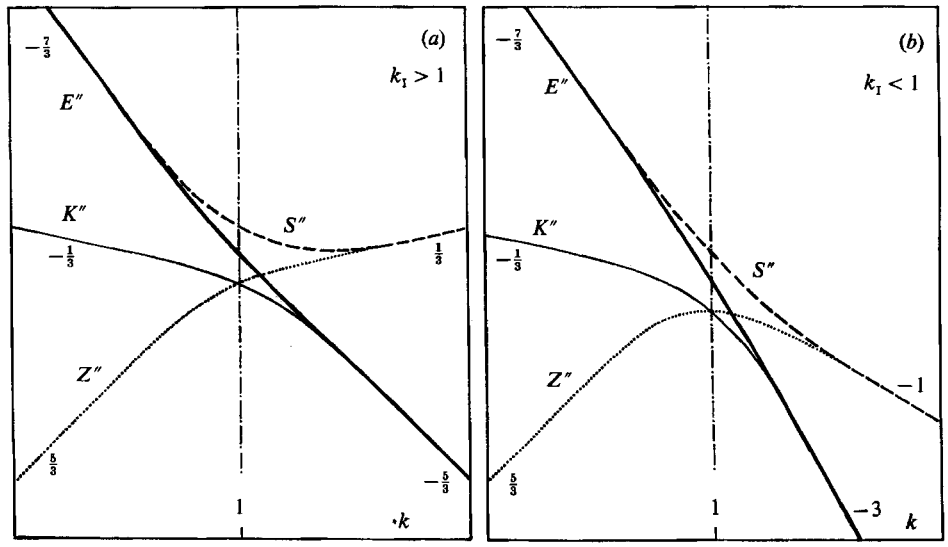

FIGURE 1. Predicted spectra of total energy E'' (———), kinetic energy K'' (———), potential enstrophy S'' (– – –) and kinetic enstrophy Z'' (· · · ·) for a quasi-geostrophic flow: (*a*) inhibition of the reverse energy cascade by a moderate rotation rate when energy and potential enstrophy are injected at wavenumber k_I larger than the Rossby deformation radius 1; (*b*) inhibition of the direct enstrophy cascade by a high rotation rate when energy and potential enstrophy are injected at wavenumber k_I smaller than the Rossby deformation radius 1.

significantly affects the dynamics of the flow; in the limit $k \ll 1$, we obtain the following asymptotic forms valid for fast rotation rates ($k_I \ll 1$):

$$\left.\begin{aligned} E''(k) &\sim \epsilon^{\frac{2}{3}} k^{-\frac{7}{3}} \quad (k < k_I) \\ E''(k) &\sim \eta^{\frac{2}{3}} k^{-\frac{7}{3}} \quad (k > k_I) \end{aligned}\right\} \tag{32}$$

and not $E''(k) \sim \eta^{\frac{2}{3}} k^{-\frac{11}{3}}$ (Farge & Sadourny 1986*a*). The spectral shape is identical in both inertial ranges, as S'' and E'' reduce to a single invariant quantity for $k \ll 1$. However, we have seen earlier that potential enstrophy dissipation in this case becomes negligible: $\eta = k_I^2 \epsilon \ll \epsilon$. Practically all the injected potential enstrophy is transferred to large scales along with energy. In other words, fast rotation inhibits the potential enstrophy cascade by strongly reducing the cascade rate.

Figure 1 (*a*, *b*) shows the shapes of the various spectra associated with (28), (30), as deduced from one another by relations (19), (20), (21). In figure 1 (*b*), the increased slope of S'' in the rotation-sensitive range ($-\frac{7}{3}$ instead of -1) reflects the inhibition of the potential enstrophy cascade by fast rotation: less potential enstrophy is reaching the small scales. In figure 1 (*a*), the collapse of kinetic enstrophy at scales larger than the radius of deformation means that rotation also inhibits the reverse energy cascade by increasing the nonlinear transfer time; a smaller amount of kinetic energy reaches the large scales than in the non-rotating case (slope $-\frac{1}{3}$ instead of $-\frac{5}{3}$); and further, the reverse cascade must bring an adequate amount of potential energy to feed the steeper ($-\frac{7}{3}$) total energy spectrum, which slows the process even more. At slow rotation rates, the inhibition of the reverse cascade occurs only when the radius of deformation is reached (figure 1*a*). At fast rotation rates, the classical energy inertial range totally vanishes, the reverse energy cascade is inhibited right from the injection wavenumber (figure 1*b*).

4. General remarks on wave–vortex interactions

We now consider the full Saint-Venant equations, and suppose that ϕ is small enough to ensure that E' and S' are close approximations to E and S. It follows from (22) that, just like in the quasi-geostrophic case, direct dissipation of potentio–vortical energy is not allowed: otherwise we would get an infinite rate of dissipation for potential enstrophy. The situation is, however, more complex than in the quasi-geostrophic case. The inertio–gravitational modes are not subject to the potential enstrophy conservation constraint: inertio–gravitational energy is therefore allowed to cascade towards small scales, where it can be dissipated. Potentio–vortical energy, on the other hand, even though it cannot be dissipated directly, may be converted into inertio–gravitational modes, being then subject to cascade and (indirect) dissipation.

Warn (1986) has studied the inviscid statistical equilibria which are solutions of (1) in the weak perturbation limit, when $E' = E$, $S' = S$ to first order. The equilibrium spectra are obtained in terms of the energy and potential enstrophy distributions (10)–(13); they generalize the classical equilibrium solutions of inviscid truncated two-dimensional flow, as obtained for instance by Kraichnan (1967), Fox & Orszag (1973) or Basdevant & Sadourny (1975). There is of course a strong similarity between the two cases, due to the correspondence between quadratic invariants. For each wavevector $\boldsymbol{k}$, we have three eigenmodes: one potentio–vortical mode, denoted by V, and two inertio–gravitational modes, denoted by G^+ and G^-. The ratios of potential enstrophy to energy, specific to each mode, are the following:

$$\mathscr{K}^2_{\mathrm{V}}(\boldsymbol{k}) = 1 + k^2, \quad \mathscr{K}^2_{\mathrm{G}^+}(\boldsymbol{k}) = \mathscr{K}^2_{\mathrm{G}^-}(\boldsymbol{k}) = 0. \tag{33}$$

The equilibrium solutions read (Warn 1986)

$$\mathscr{E}'_X(\boldsymbol{k}) = (\alpha + \beta \mathscr{K}^2_X(\boldsymbol{k}))^{-1}, \tag{34}$$

with X equal to either V, G^+ or G^-. The formula is formally like in the incompressible case, α and β being uniquely determined from a given choice of the linearized invariants E' and S' (for an exact demonstration, see Sadourny 1985); (34) can be rewritten using (33)

$$\mathscr{E}'_{\mathrm{V}}(\boldsymbol{k}) = (\alpha + \beta(1+k^2))^{-1}, \quad \mathscr{E}'_{\mathrm{G}}(\boldsymbol{k}) = 2/\alpha. \tag{35}$$

The important consequence of (35) is the systematic dominance of inertio–gravitational energy at all wavenumbers, at least when β is positive, which is always the case for high enough resolutions. This means that shallow-water dynamics might *a priori* be able to convert, at least to some extent, potentio–vortical energy into inertio–gravitational energy, which supports the possibility, already mentioned, of systematic indirect dissipation of rotational energy in the limit of infinite Reynolds numbers.

5. Numerical experiments

The numerical experiments presented here have been performed using the pseudospectral model that we have developed directly on form (1) of the Saint-Venant equations. The initial-value problem is solved on a doubly periodic plane, using the Temperton (1983) very fast Fourier transform algorithm, with $N^2 = 128^2$ real degrees of freedom in spectral space. An additional circular truncation is imposed at wavenumber 64, in order to secure a quasi-isotropy of the smaller scales.

The time integration is done with an explicit leapfrog scheme for the conservative terms, and an exact integration for the dissipation term when it is added to (1). In order to follow the dynamics of the fastest inertio–gravity waves with an acceptable amount of numerical dispersion errors, we choose a time step equal to 0.75 times the maximum value allowed by the Courant–Friedrichs–Lewy (CFL) stability criterion applied to the fastest inertio–gravity waves; this time step is indeed much smaller than the smallest eddy-turnover time. To initialize the leapfrog scheme, we solve the linearized equations (5) using a normal-mode integration, which is reasonable because nonlinear effects have not yet developed during the first time step, much smaller than the eddy-turnover time. As soon as the separation between the odd and even solutions exceeds 10%, owing to the excitation of the leapfrog numerical mode by some nonlinearities, we restart the calculation from one of the two last solutions with the same procedure as used for the initial step. This is actually only necessary when the rotational eddies strongly dominate the inertio–gravitational waves, i.e. for two cases (balanced initial flows) out of six. The computation of one time step requires 58 ms on a Cray 1-S and a typical integration, done during 100000 time steps, is of the order of 1.6 hours.

When numerically integrating the Saint-Venant equations, we have to face two basic difficulties: first, the aliasing problem due to nonlinearity, and secondly, the behaviour of the non-quadratic invariants such as energy and potential enstrophy. In the pseudospectral approach used here, an M^2-point grid in physical space is associated with N^2 modes in real spectral space. Nonlinear energy is strictly conserved when $M = N$, at the expense of aliasing errors; when $M = \frac{3}{2}N$, aliasing is suppressed, but nonlinear energy is no longer conserved (Farge & Lacarra 1988). Concerning the nonlinear potential enstrophy, it is not conserved for a finite number of modes. In the incompressible case, where invariants are quadratic, Parseval's theorem yields a natural decomposition of the flow into its various spatial scales; further, energy is then strictly conserved in any truncated system under the dynamics of triadic interactions. In the present compressible two-dimensional case, as we have seen above, there is no unequivocal energy decomposition into spatial scales. Accordingly energy conservation is not a natural property of the truncated system, even though it remains an asymptotic property for strictly inviscid flows in the limit of infinite resolution. In fact, we have preferred to allow aliasing errors and formally conserve energy, for the following reasons: energy conservation (2) is indeed an efficient asymptotic constraint on the solution, easy to check in the course of computation; further, the aliasing problems seem to be not so harmful in turbulent flow simulations as soon as spectral slopes are steep enough or strongly damped near the cut-off scale, the folding of small-scale energy having then a truly negligible effect on the large scale; lastly, the desaliasing procedure is computationally very expensive because it requires $1.5N$ grid points instead of N. We have checked the energy conservation of our scheme by running several inviscid computations; we found that energy is conserved within 0.3% during 100000 time steps.

The simulation of fully developed turbulence, in decaying or forced conditions, raises the problem of modelling the effect of the subgrid-scale structures, insofar as the dissipative scales are not explicitly described owing to insufficient resolution. For two-dimensional motion like shallow-water flows, molecular dissipation in $\nu\nabla^2$, ν being kinematic viscosity, is not necessarily a relevant model of the actual small-scale dissipation, which should rather be described as a transition from two-dimensional to three-dimensional motion before reaching the scales where dissipation actually occurs. The practical problem of subgrid-scale parametrization within an

inertial range has already received a great deal of attention in the incompressible case, where the use of a highly selective 'hyper-dissipativity' operator, of the form

$$-\nu(-\nabla^2)^\alpha, \tag{36}$$

with large values of α, has proven to be adequate (Basdevant *et al.* 1981; McWilliams 1984; Roy 1986). The higher the exponent, the smaller the ratio of energy dissipation to enstrophy dissipation; the use of (36) with large values of α thus guarantees an almost vanishing rate of energy dissipation, as predicted by the theory of two-dimensional turbulence for the incompressible case. Even more sophisticated diffusion operators have been designed, in which energy is strictly conserved (Sadourny & Basdevant 1985); but, for the full Saint-Venant equations, we are yet lacking a comprehensive theory of nonlinear interactions in order to derive an adequate subgrid-scale parametrization in this context. The only *a priori* desirable property is that subgrid-scale modelling should reduce to a highly selective form like (36) in the absence of inertio–gravitational motion; we shall therefore choose to use (36), with $\alpha = 8$, applied to all variables (velocity and geopotential).

The choice of dissipating all dependent variables equally is the simplest one, whose validity can only be judged on the grounds of numerical results to be discussed later. First, it is not obvious that we have to dissipate the free-surface geopotential in the same manner as we dissipate the velocity components. This choice may even appear unphysical since geopotential can be interpreted here as a two-dimensional density. Subgrid-scale parametrization, however, is very different from molecular diffusion: we expect that the mixing by velocity gradients must diffuse all perturbations, including those of the free-surface height, and therefore avoid the appearance of singularities due to wave breaking. In any case, diffusing all dependent variables in the same manner appears at least consistent with our desire to dissipate shallow-water flows like incompressible flows in the quasi-geostrophic limit, the potential vorticity modes being defined as a linear combination of vorticity and geopotential.

For quasi-geostrophic flows, dominated by rotational motion, we shall define a 'turbulent' viscosity coefficient ν_Z appropriate to the rotational dynamics such that

$$\nu_Z = \tau_Z^{-1} k_{\max}^{-2\alpha} \tag{37}$$

with τ_Z inversely proportional to the square-root of the kinetic enstrophy Z:

$$Z = \frac{1}{2}\iint (\boldsymbol{N}\cdot(\boldsymbol{\nabla}\times\boldsymbol{V}))^2 \,\mathrm{d}x\,\mathrm{d}y. \tag{38}$$

But, owing to the presence of inertio–gravity waves and the associated divergent motions, we have to adjust ν, not only in terms of the kinetic enstrophy Z, i.e. a measure of velocity gradients limited to the rotational part of the flow, but also in terms of the divergent component of the flow. For instance, if we consider a purely divergent flow, we can write the equations for the geopotential and the velocity potential in spectral form:

$$\left.\begin{aligned} \frac{\partial\phi}{\partial t}\bigg|_{-k} - \omega_k^2\chi_{-k} + \sum_S \boldsymbol{k}\cdot\boldsymbol{q}\phi_p\chi_q = 0, \\ \frac{\partial\chi}{\partial t}\bigg|_{-k} + \phi_{-k} - \sum_S \boldsymbol{p}\cdot\boldsymbol{q}\chi_p\chi_q = 0, \end{aligned}\right\} \tag{39}$$

Σ_S being a symmetrized sum over all non-ordered couples $(\boldsymbol{p},\boldsymbol{q})$. If we exclude the linear coupling terms, these equations have a structure similar to the vorticity

equation, from which we may infer a characteristic nonlinear timescale τ_D whose square is inversely proportional to the integral of divergence squared:

$$D = \frac{1}{2}\iint (\nabla \cdot \boldsymbol{V})^2 \,\mathrm{d}x\,\mathrm{d}y. \tag{40}$$

Then we may construct a 'turbulent' viscosity coefficient appropriate to purely divergent dynamics:

$$\nu_D = \tau_D^{-1} k_{\max}^{-2\alpha}. \tag{41}$$

In the general case, where we have a mixture of rotational and divergent motions, we shall then define a generalized turbulent viscosity coefficient:

$$\nu = \nu_Z + \nu_D. \tag{42}$$

We perform six numerical experiments realized under conditions similar to those of the terrestrial atmospherical flow:

size of the periodic domain	L	6400 km,
mean free-surface height	H	10 km,
i.e. mean geopotential	$\langle \Phi \rangle = (gH)^{\frac{1}{2}}$	10^5 m^2 s^2,
geopotential fluctuations	ϕ	1–5 % of $\langle \Phi \rangle$,
mean velocity		0 m s^{-1},
velocity fluctuations	$\lvert \boldsymbol{V} \rvert$	5–20 m s^{-1}.

The initial fields are chosen as Gaussian random realizations for each Fourier component, the variance of each wavevector being a given function of the wavenumber, with a maximum of excitation at $k_I = 3$. These six experiments differ by the choice of both initial conditions and rotation rates. We consider three different initial flows, characterized by various levels of inertio–gravitational energy. The first is a flow (referred to as B), for which divergence and time derivative of divergence are initially set equal to zero, by solving

$$\nabla^2(\phi + \tfrac{1}{2}V^2) = \boldsymbol{N} \cdot \nabla \times [(1 + \boldsymbol{N} \cdot (\nabla \times \boldsymbol{V}))\, \boldsymbol{V}]; \tag{43}$$

this flow is in nonlinear balance and therefore the initial motion is nearly incompressible, i.e. strongly dominated by geostrophic vortices with only a negligible amount of inertio–gravity waves. This limit case is used to check and compare our model to the well-known behaviour of decaying two-dimensional incompressible turbulent flows (McWilliams 1984). The second initial flow (referred to as R) is mostly rotational and presents a mixture of geostrophic vortices and inertio–gravity waves. The third flow (referred to as I) is purely irrotational and strongly dominated by inertio–gravity waves with only a small amount of potentio–vortical energy contained in the geopotential field. We compute each of these initial flows with two different rotation rates: either a moderate rotation (referred to as M) with $f = 10^{-4}$ s^{-1}, or a high rotation (referred to as H) with $f = 6\ 10^{-4}$ s^{-1}, the corresponding Rossby deformation† being respectively $k_D = 2$ and $k_D = 12$. With this set of parameters, the Rossby number ($\langle \boldsymbol{N} \cdot (\nabla \times \boldsymbol{V}) \rangle / f$) is in the range 0.01 to 0.1, while the Mach number ($\langle \lvert \boldsymbol{V} \rvert \rangle / (gH)^{\frac{1}{2}}$) is in the range 0.03 to 0.1. Each experiment is integrated over 100000 time steps, which, with our adimensional time unit (normalized by f^{-1}), corresponds to $t_{\max} = 377$ for moderate rotation and $t_{\max} = 2262$ for high rotation.

For each of these six numerical experiments, we display the time evolution of total

† The values given here are not normalized; the normalized value of k_D is always one, according to our definitions.

potential enstrophy and total energy, split into its potentio–vortical and inertio–gravitational parts, the timescale being measured in terms of adimensional time units (figure 2). We also analyse the uni-dimensional energy spectra of both potentio–vortical and inertio–gravitational energies, comparing their initial and final modal distributions (figure 3). Then, to complement to this spectral approach, we study the spatial structure of different fields in physical space, namely vorticity, divergence, stream function, geopotential and potential vorticity (figure 6). Each field is visualized with an appropriate normalized colour scale that we have designed in order to facilitate a morphological analysis of two-dimensional scalar flows and allow comparisons between different experiments (Farge 1987): warm colours correspond to positive values, cold colours to negative values while the central isoline indicates the level zero; we have superimposed a luminance scale organized in such a way that we can extract maximal information from both large and small scales. As a result enough information is kept on the black and white plates to distinguish positive structures, characterized by a clearer centre, from negative structures, characterized by a darker centre, delimited by a clear isoline in between for the separatrix zero. This approach in terms of physical space variables provides new insights to better understand the underlying dynamics, especially the formation of coherent vortices, the inertio–gravity wave behaviour and the related geostrophic adjustment process.

6. Results and discussion

6.1. *Dissipation properties*

We first note that, in all our simulations, perturbations remain small enough to yield $E \approx E' \equiv E'_{\mathrm{V}} + E'_{\mathrm{G}}$ at all times, with a relative error $|E-E'|/E$ less than 10^{-3}. This, *a posteriori*, justifies our analyis in terms of potentio–vortical and inertio–gravitational energies, corresponding to the normal eigenmodes of the linearized Saint-Venant equations (5). The evolution of S', E', E'_{V} and E'_{G} is shown in figure 2. When the velocity and mass fields are initially in balance equilibrium, energy is in practice exactly conserved (it decreases by less than 1 % throughout the integrations), while potential enstrophy is strongly dissipated and decreases by an order of magnitude (figure 2*a*, *b*). This is of course consistent with the well-known behaviour of quasi-geostrophic, or incompressible, two-dimensional turbulent flows; a further look at the energy partition into potentio–vortical and inertio–gravitational components confirms that the flow remains in balance equilibrium at all times. More generally, we do not observe, in any of our six experiments, significant energy exchanges between the inertio–gravitational and the potentio–vortical parts of the motion: potentio–vortical energy is always conserved throughout the integration, irrespective of the rotation rate and of the inertio–gravitational energy level, just like in quasi-geostrophic flow. It seems that, in the case of small geopotential fluctuations studied here, the dynamics of inertio–gravitational modes and potentio–vortical modes are to a large extent decorrelated. This behaviour contradicts the prediction, made on the grounds of statistical equilibria, that potentio–vortical energy, if it is large enough, should tend in the long term to feed the inertio–gravitational part of the flow; the two conclusions, however, could be reconciled if the relaxation timescales towards statistical equilibria are large compared with the dissipation timescales of the present experiments.

The dissipation of potential enstrophy appears sensitive to the rotation rate (figure

	B	R	I
M	8.82	11.3	93734
H	8.31	72.3	312327

TABLE 1. Ratio $\tau_S(t_0)/\tau_Z(t_0)$ for the six different experiments

2). We may define the potential enstrophy dissipation rate, averaged between times t_0 and t_1 close to t_0, as

$$\tau_S(t_0) = \frac{t_1 - t_0}{1 - [S(t_1)/S(t_0)]}. \tag{44}$$

For t_1 close enough to t_0, this observed dissipation rate can be compared to the phenomenological estimate $\tau_Z(t_0) = [Z(t_0)]^{-\frac{1}{2}}$ of incompressible two-dimensional turbulence. Table 1 shows the ratio τ_S/τ_Z at the initial time t_0 of the different simulations. In the balance case (B) we expect a behaviour close to two-dimensional incompressible flow, and therefore insensitive to rotation. Table 1 confirms that, near the initial time, $\tau_Z(t_0)$ is a good estimate of $\tau_S(t_0)$ up to a multiplicative constant which is indeed independent of rotation. However, at large times, we observe a marked inhibition of the enstrophy dissipation in the fast-rotation case, which is consistent with our prediction of §3. The same type of inhibition is also visible on figure 2 for the rotational case (R), but figure 2 and table 1 together show that the initial decay rate of potential enstrophy becomes weaker as the initial level of inertio–gravitational energy increases: the presence of inertio–gravity waves actually makes the enstrophy cascade process less efficient. As we have seen before, there is no energy exchange taking place between inertio–gravitational and potentio–vortical modes; the mechanism involved in the inhibition of potential enstrophy by inertio–gravity waves must be of another kind. The quantity that cascades is potential enstrophy, which is globally conserved by the nonlinear processes. However, the efficiency of the cascade is measured by the kinetic enstrophy, as it is the kinetic part of the flow that actually exerts the straining of potential vortices (cf. §3). By definition the potential vorticity field is free from inertio–gravity waves, consequently it is the kinetic vorticity field that loses its coherency when inertio–gravity waves are present (this effect is particularly conspicuous by comparing the vorticity and potential vorticity fields on figure 6*e*), and the resulting loss of coherency of the straining mechanism causes an inhibition of the cascade process.

Figure 2 also shows a total inhibition of inertio–gravitational energy under the effect of rotation. In the absence of rotation, the inertio–gravity waves are not dispersive, and any mode can have resonant interaction with any other leading to an energy dissipation in the small scales (*c*, *e*). But under the effect of rotation, namely for scales $k < 1$, the inertio–gravity waves become dispersive and then triadic interactions are no longer feasible. We therefore observe no inertio–gravitational energy dissipation (*d*,*f*). This inhibition process will be discussed in §6.4.

6.2. *Potentio–vortical energy spectra*

Energy spectra are displayed in figure 3. In all cases the potentio–vortical energy spectrum approximately follows a law in k^{-4}. This is not surprising for flows initially

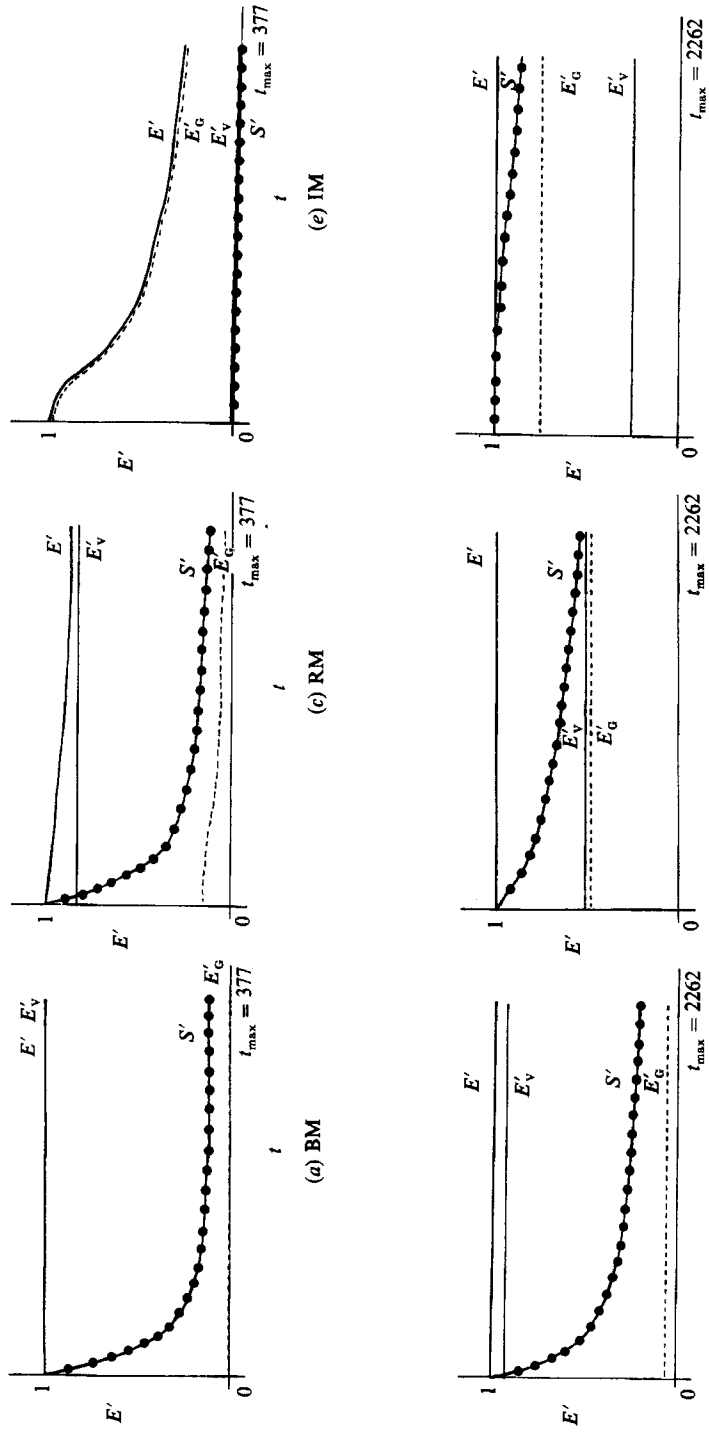

FIGURE 2. Time evolution, from $t = 0$ to $t = t_{max}$, of potential enstrophy S' (—●—●—●—), total energy E' (———), potentio–vortical energy E'_V (———) and inertio–gravitational energy E'_G (– – –), for the six experiments.

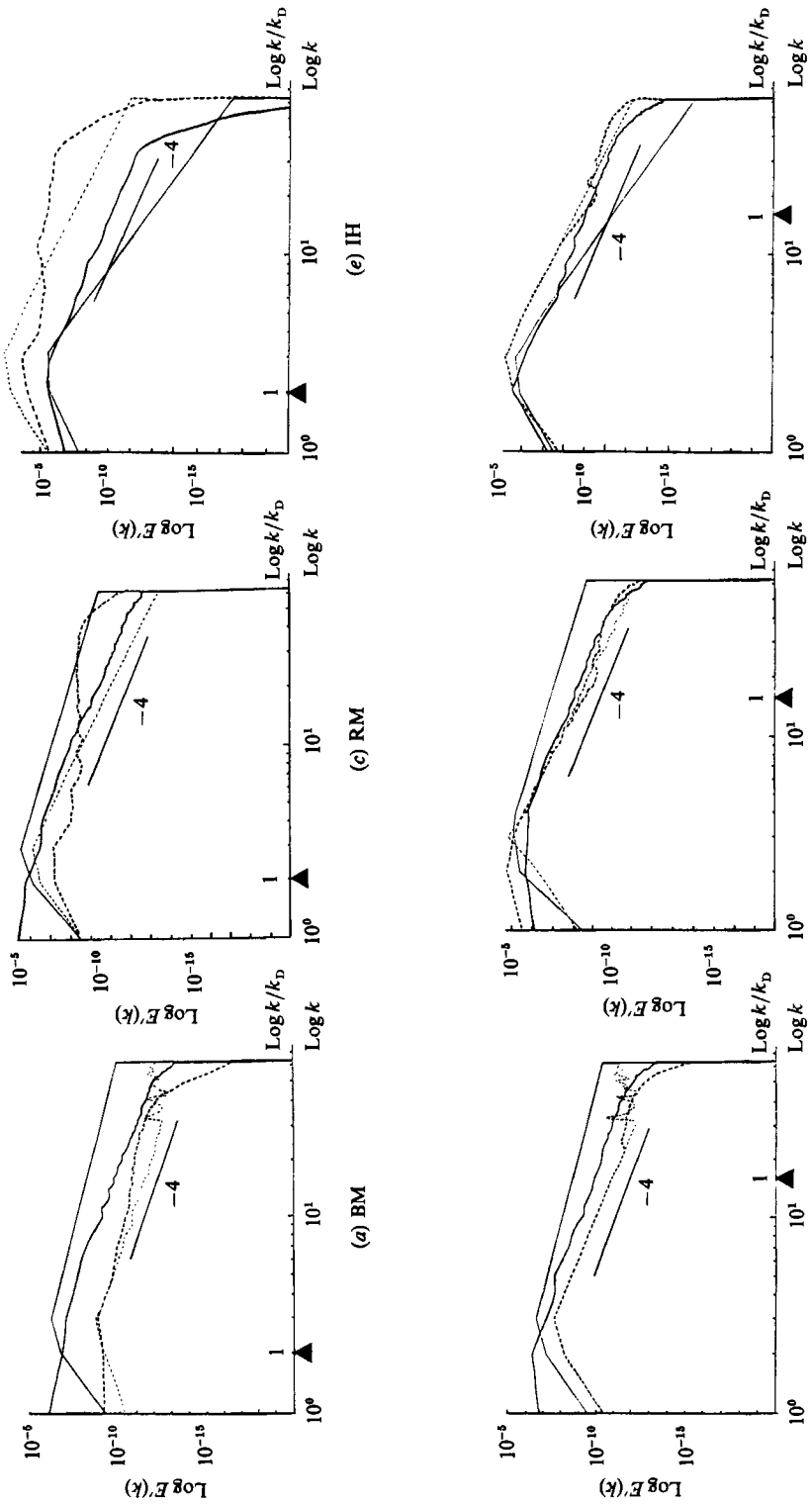

FIGURE 3. Unidimensional spectra, at $t = 0$ (thin lines) and $t = t_{max}$ (thick lines), of potentio–vortical energy (——) and inertio–gravitational energy (- - - - - -) for the six experiments. The triangle indicates the Rossby deformation wavenumber.

in balance equilibrium, where the motion remains approximately balanced (i.e. quasi-incompressible) for all times: such laws have often been observed in numerical simulations of decaying or forced two-dimensional turbulence at similar resolutions (Basdevant *et al.* 1981; Bennett & Haidvogel 1983; McWilliams 1984). The additional information in figure 3 is that the spectral law, in k^{-4}, is not destroyed by the presence of inertio–gravitational modes, even strongly excited. Similarly, in the statistical equilibrium case, we have observed that the equipartition of potential enstrophy at small scales is not perturbed by the equipartition of inertio–gravitational energy, even though inertio–gravitational excitation strongly dominates. Sadourny (1975), studying inviscid shallow-water motion in low-resolution numerical models, also found such independent equipartitions in the smaller scales, although his simulations were not long enough to reach statistical equilibria; in his case too, the inertio–gravitational modes were far more energetic than the potentio–vortical modes at small scales.

6.3. *Isolated coherent vortices*

An interesting point about the behaviour of the rotational part of the flow is the presence or absence of isolated coherent vortices in the vorticity field, emerging out of a background of elongated vorticity filaments. Concerning incompressible two-dimensional turbulence, such condensation of the vorticity field into isolated coherent vortices is found very systematically in long-term numerical simulations at comparable resolutions, in both decaying and forced conditions (Fornberg 1977; Basdevant *et al.* 1981; McWilliams 1984; Babiano *et al.* 1987). They are relatively stable structures, which dominate the turbulent medium in between by at least an order of magnitude; they emerge from the flow by some phase-locking process and survive for very long lifetimes compared with the timescale of nonlinear transfers in the fluid, namely the averaged eddy-turnover time.

Figures 4(*a*, *b*) (plate 1) shows that the vortex cores are the least regular (in the sense of Hölder regularity, i.e. are described by functions having high-order derivatives which do not vanish) features in the vorticity field. The background flow in between vortices is not only less excited, but also more regular. This tends to contradict the classical interpretation of two-dimensional turbulent flows (McWilliams 1984): the smallest scales of the vorticity field are not the filamentary structures, which get formed at the vortex periphery under the action of the enstrophy cascade, but are concentrated inside the vortex cores. This has been confirmed (Farge & Rabreau 1988) by performing a wavelet analysis, i.e. a space-scale decomposition, of a vortex section within a vorticity field from experiment BM (figure 5). Dissipation, which is proportional to the Laplacian of vorticity, and is therefore sensitive to the small scales, would thus act not only on vorticity filaments but also on the internal structure of vortices, where this Laplacian is the strongest (figure 4*c*, plate 1). The presence of very small scales in the vortex cores cannot be explained by local vortex stretching, because the vorticity fields shown on figure 4 and analysed on figure 5 correspond to initially balanced flows, remaining in balance equilibrium during their evolution, which therefore behave as incompressible two-dimensional flows. This excitation of the internal structure of vortices may impair the contour-dynamics approach (Zabusky 1984; Dritschel 1986) to explaining the behaviour of turbulent flows, because this technique freezes, or at least limits (in the case of multicontours), the number of degrees of freedom internal to the vortices.

In the shallow-water case, isolated coherent vortices seem to develop only when the level of excitation of inertio–gravitational waves is low, i.e. in three cases out of

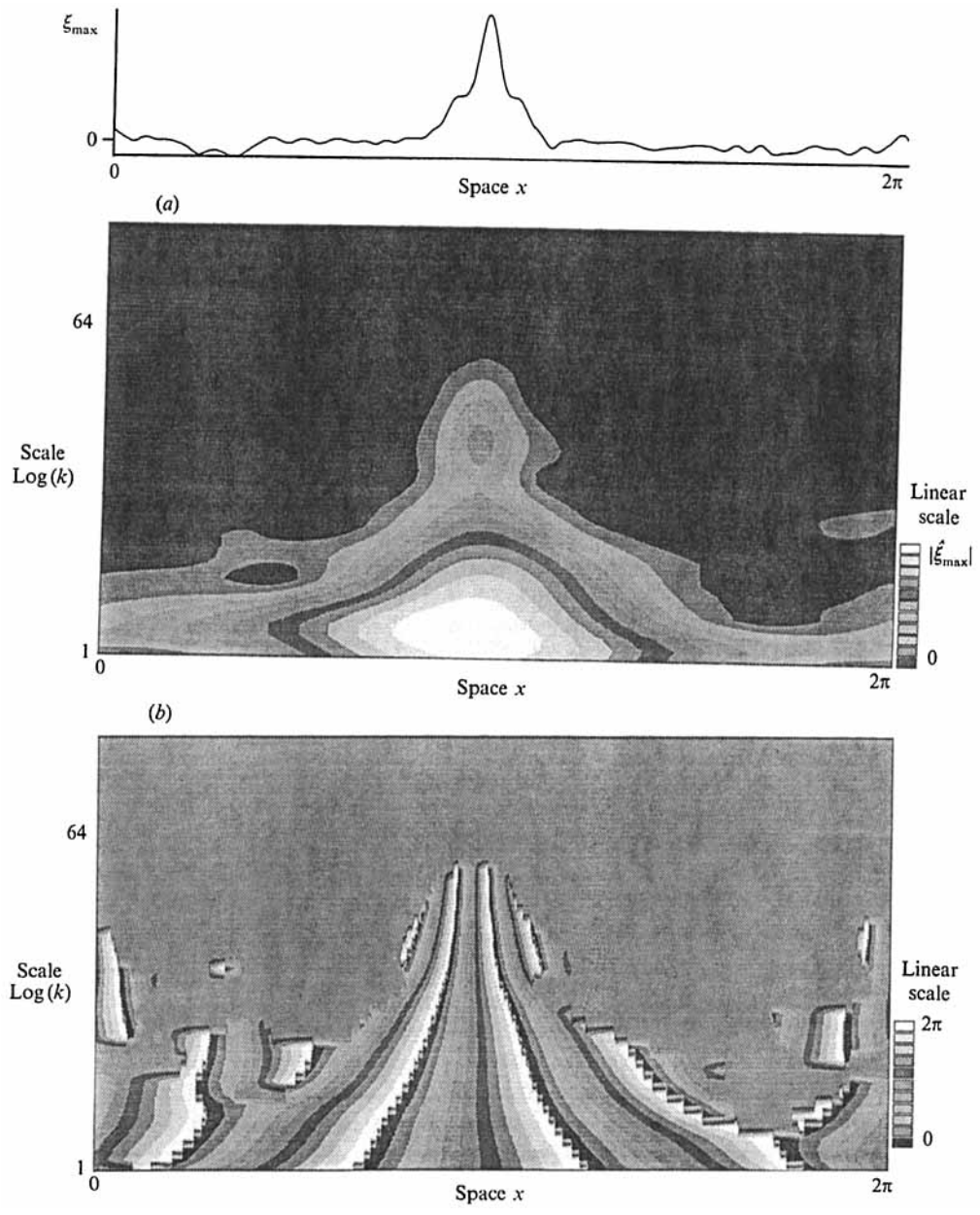

FIGURE 5. Wavelet transform of a one-dimensional cut in the vorticity field for a flow in balance equilibrium with moderate rotation, experiment BM at $t_{max} = 377$: (*a*) modulus of the complex wavelet coefficients; it gives the space-scale decomposition of the enstrophy and we observe that the smallest scales are confined in the vortex core; (*b*) phase of the complex wavelet coefficients; the lines of constant-phase point towards the most irregular part of the signal and we see that it corresponds to the vortex core.

six (figure 6*a* (plate 2), and figure 6*b*, *c*). This suggests that both the direct potential enstrophy cascade, characterized by the filamentation of the vorticity field, and the inverse rotational energy cascade, characterized by the formation of large-scale coherent structures through the merging of same-sign vortices, are reduced under the action of inertio–gravity waves. We also observe that a stronger contrast between the isolated vortices and the turbulent background is obtained when the rotation rate is moderate (figure 6*a*, *c*), which shows a similar inhibition of the nonlinear cascades due to rotation: even in the balance case, where inertio–gravitational waves are negligible, the contrast weakens when rotation increases (figure 6*a*, *b*), an effect consistent with the inhibition already mentioned in §6.1. The other extreme is the case of a flow dominated by inertio–gravitational waves at moderate rotation rates. There, we observe a random wave-like structure of the vorticity field, more characteristic of short-scale inertio–gravitational waves than of ordinary turbulence (figure 6*e*). The intermediate cases are those of flows presenting comparable amounts of potential vortices and inertio–gravitational waves, but subject to fast rotation (figure 6*d*, *f*): there, the vorticity field is organized into elongated, one-dimensional sheets of alternating sign, wrapped around one another; but again isolated coherent vortices are missing.

Indeed, we find that the same k^{-4} spectrum (figure 3) covers a wide variety of structures for the vorticity field in physical space (Farge & Sadourny 1986*b*). At moderate rotation rate, the dominance of inertio–gravitational energy induces a random wave-like structure at small scales (figure 6*e*); but at high rotation rates, we observe a distribution of vorticity sheets consistent with Saffman's (1971) hypothesis (figure 6*f*). When the inertio–gravitational wave level is weak, the k^{-4} spectrum is associated with a distribution of coherent vortices (figure 3*a*, *b*, *c*). The persistence of the same spectral law, whatever the structure of the vorticity field, appears indeed remarkable and tends to prove the incompleteness of the Fourier spectral analysis in handling such problems, where the coherence of the flow may be an essential dynamical feature. This is why we also consider the wavelet spectral analysis, which gives a local scale decomposition or, in other words, a local spectrum (figure 5).

The true potential vorticity q, (3), generalizes the linearized potential vorticity q', (9), and thus, contrary to vorticity, can be considered free of an inertio–gravitational component. Therefore, in the analysis of shallow-water flows, potential vorticity gives us direct information on the potentio–vortical part of the flow and the related potential enstrophy cascade. For instance, an intense potential enstrophy cascade is recognized by a low level of excitation between isolated potential vortices (figure 6*a*, *b*, *c*). The weak flow there has been intensitively laminated into highly elongated filaments giving a handle to an active dissipation in the smaller scales. On the contrary, a weak or non-existent potential enstrophy cascade does not produce such a lamination; consequently potential vorticity remains highly excited everywhere, without condensing into isolated vortices (figure 6*c*, *e*, *f*).

6.4. *Inertio–gravitational energy spectra*

In contrast to the potentio–vortical energy spectra, inertio–gravitational energy spectra appear extremely sensitive to the experimental conditions, especially the rotation rate. The effect of rotation is described in terms of scales relative to the radius of deformation, which in our normalization is taken as unit length.

At scales larger than the Rossby deformation radius (for $k < 1$), the transfers involving the inertio–gravitational modes appear more strongly inhibited than their potentio–vortical counterparts. Consequently, the inertio–gravitational energy

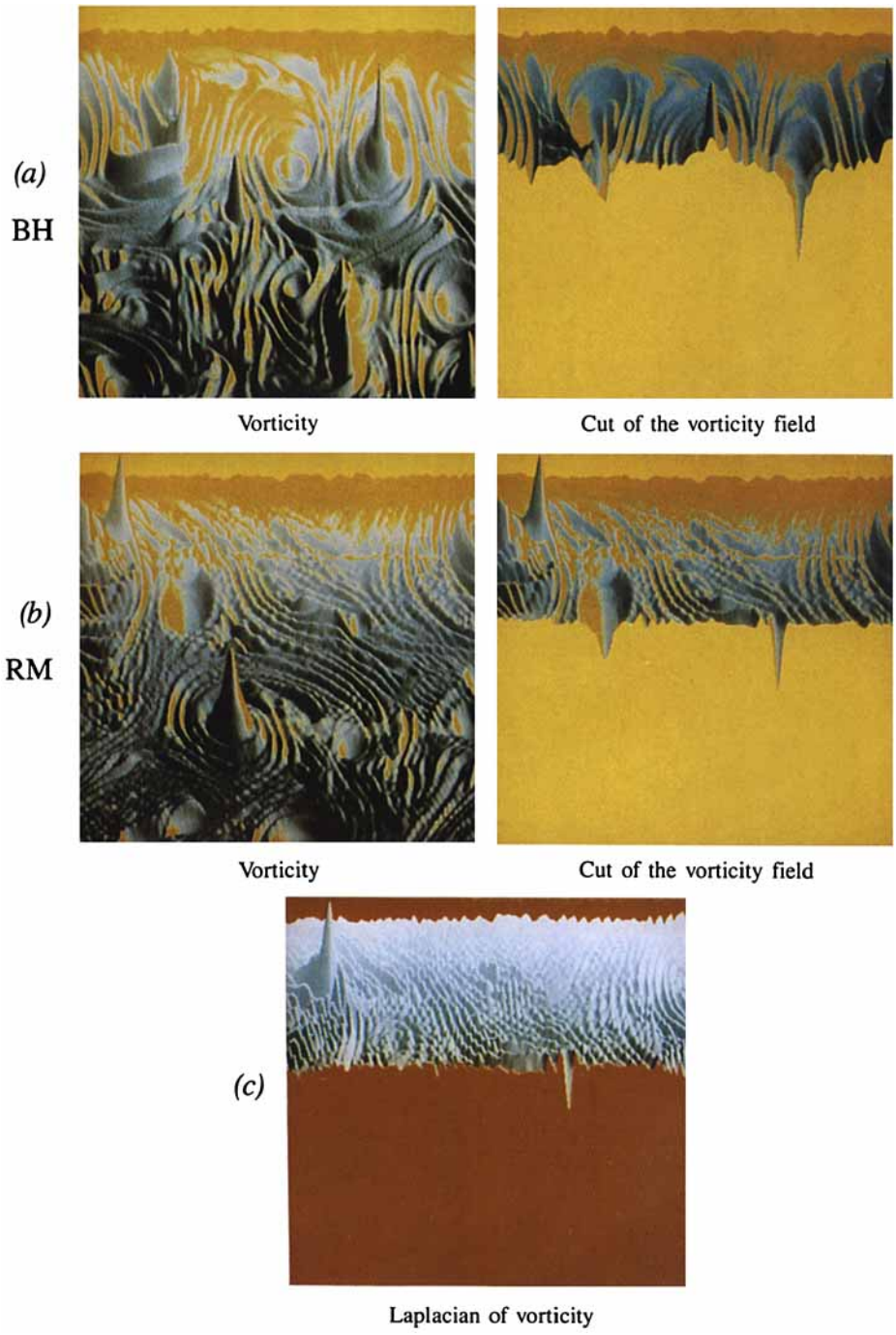

FIGURE 4. Flow structure of *(a)* the vorticity field for a flow in balance equilibrium with high rotation, experiment BH at $t_{max} = 2262$; *(b)* the vorticity field for a rotational flow with moderate rotation, experiment RM at $t_{max} = 377$; *(c)* the Laplacian of vorticity for a rotational flow with moderate rotation, experiment RM at $t_{max} = 377$.

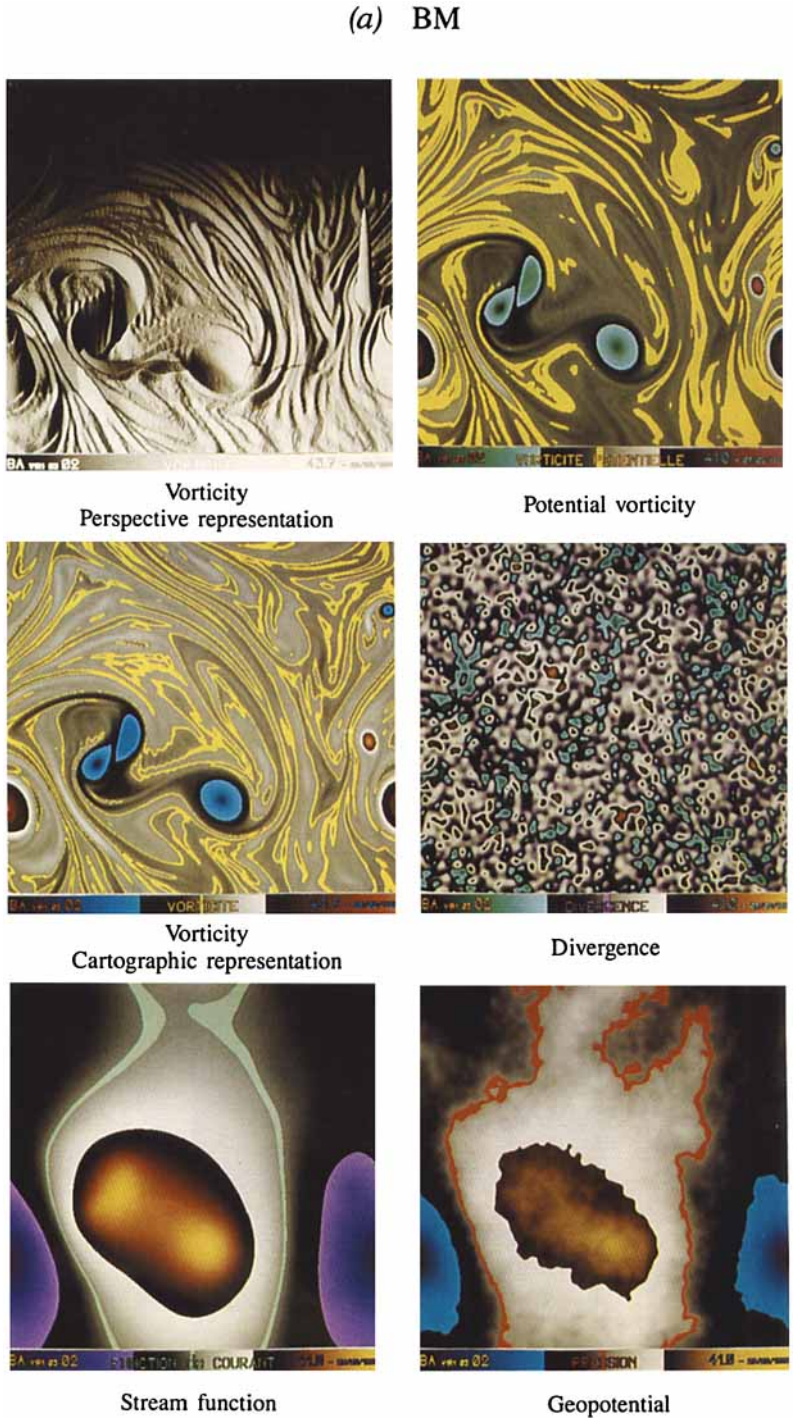

FIGURE 6*(a)*. For caption see page 455.

(*c*) RM

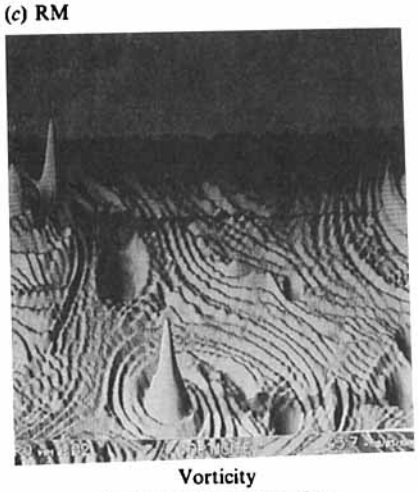

Vorticity
Perspective representation

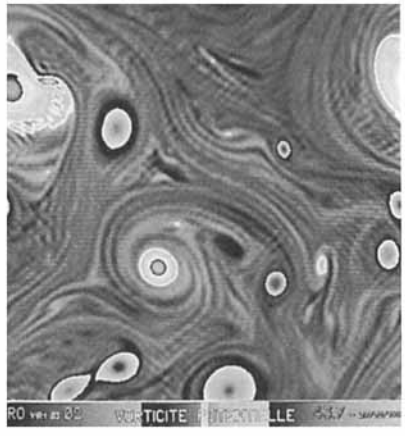

Potential vorticity

Vorticity
Cartographic representation

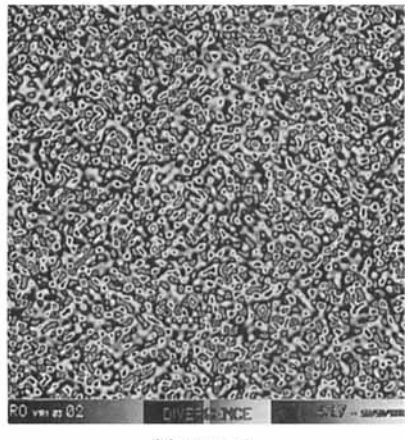

Divergence

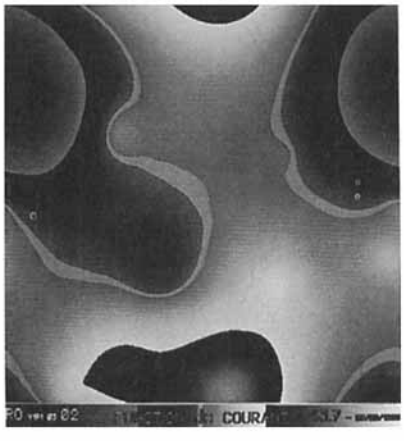

Stream function

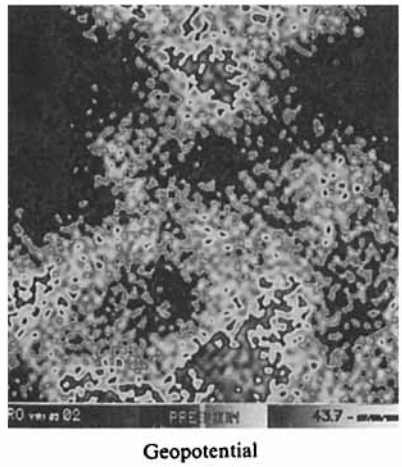

Geopotential

FIGURE 6(*b*). For caption see page 455.

(*c*) RM

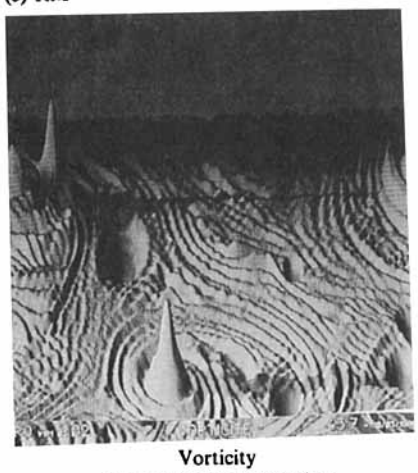

Vorticity
Perspective representation

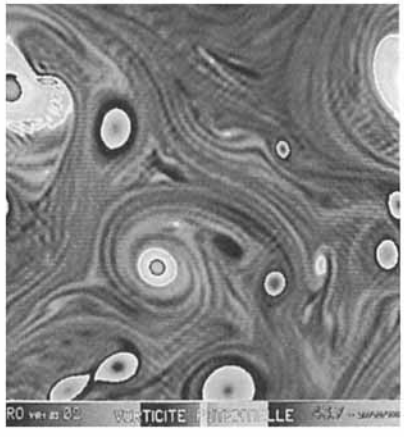

Potential vorticity

Vorticity
Cartographic representation

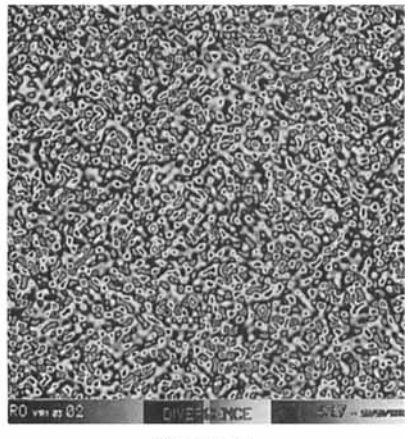

Divergence

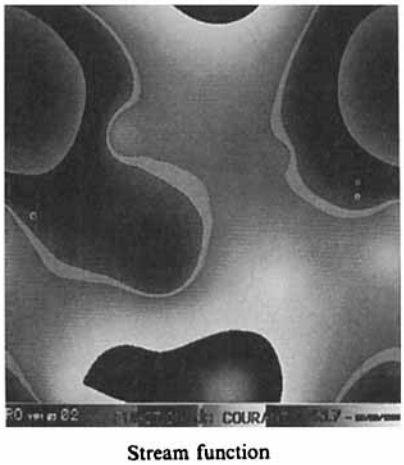

Stream function

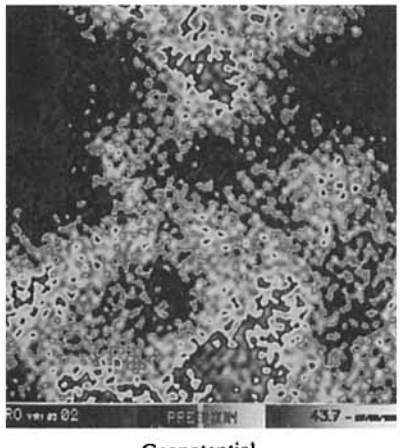

Geopotential

FIGURE 6(*c*). For caption see page 455.

(*d*) RH

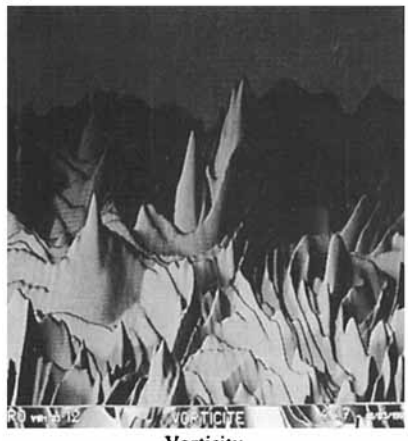

Vorticity
Perspective representation

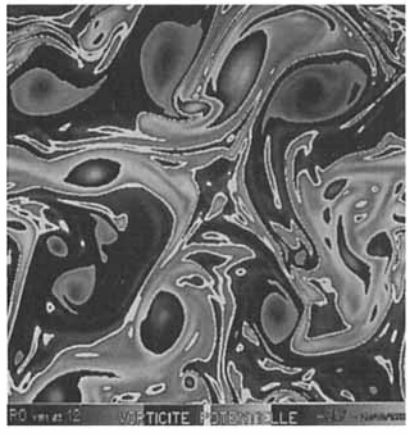

Potential vorticity

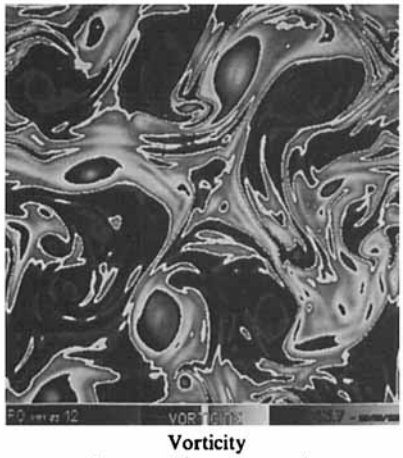

Vorticity
Cartographic representation

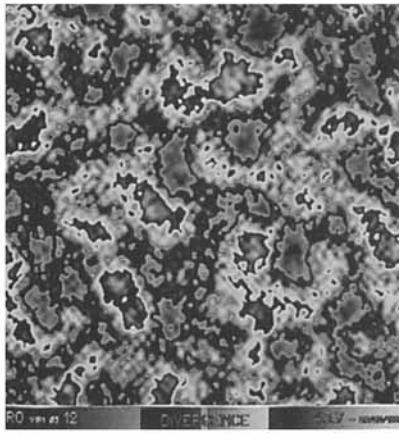

Divergence

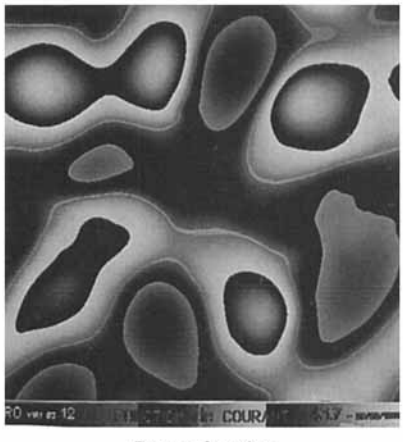

Stream function

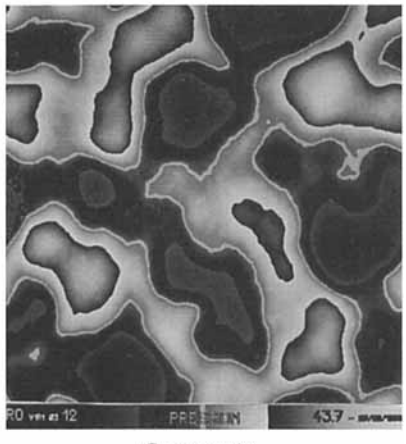

Geopotential

FIGURE 6(*d*). For caption see page 455.

(*e*) IM

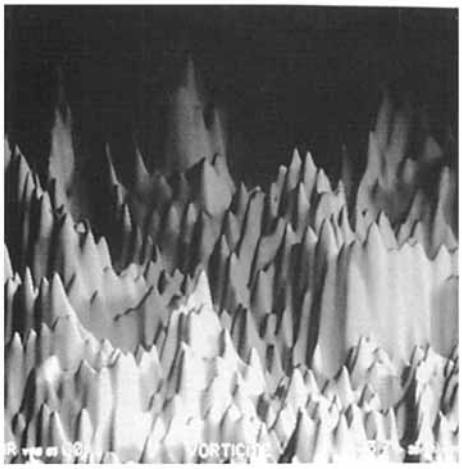

Vorticity
Perspective representation

Potential vorticity

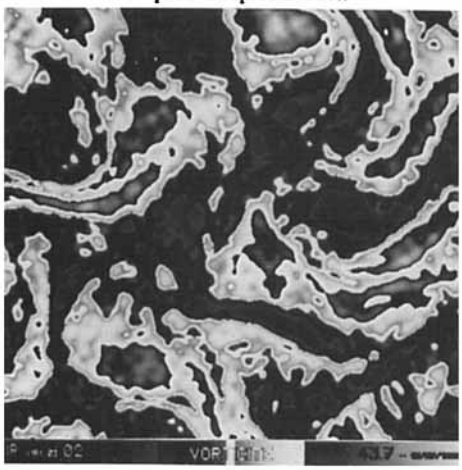

Vorticity
Cartographic representation

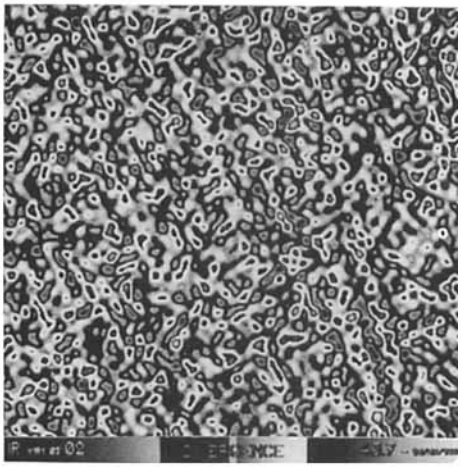

Divergence

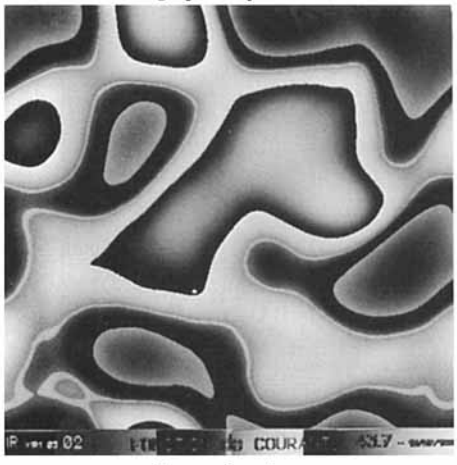

Stream function

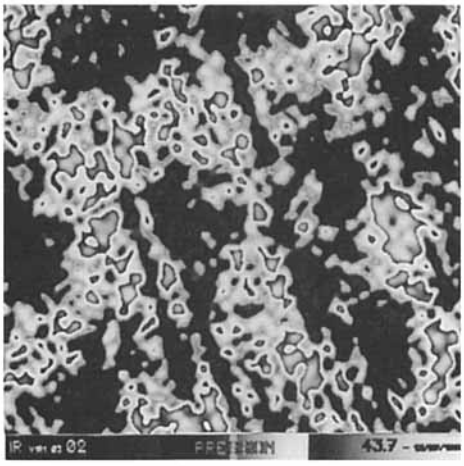

Geopotential

FIGURE 6(*e*). For caption see facing page.

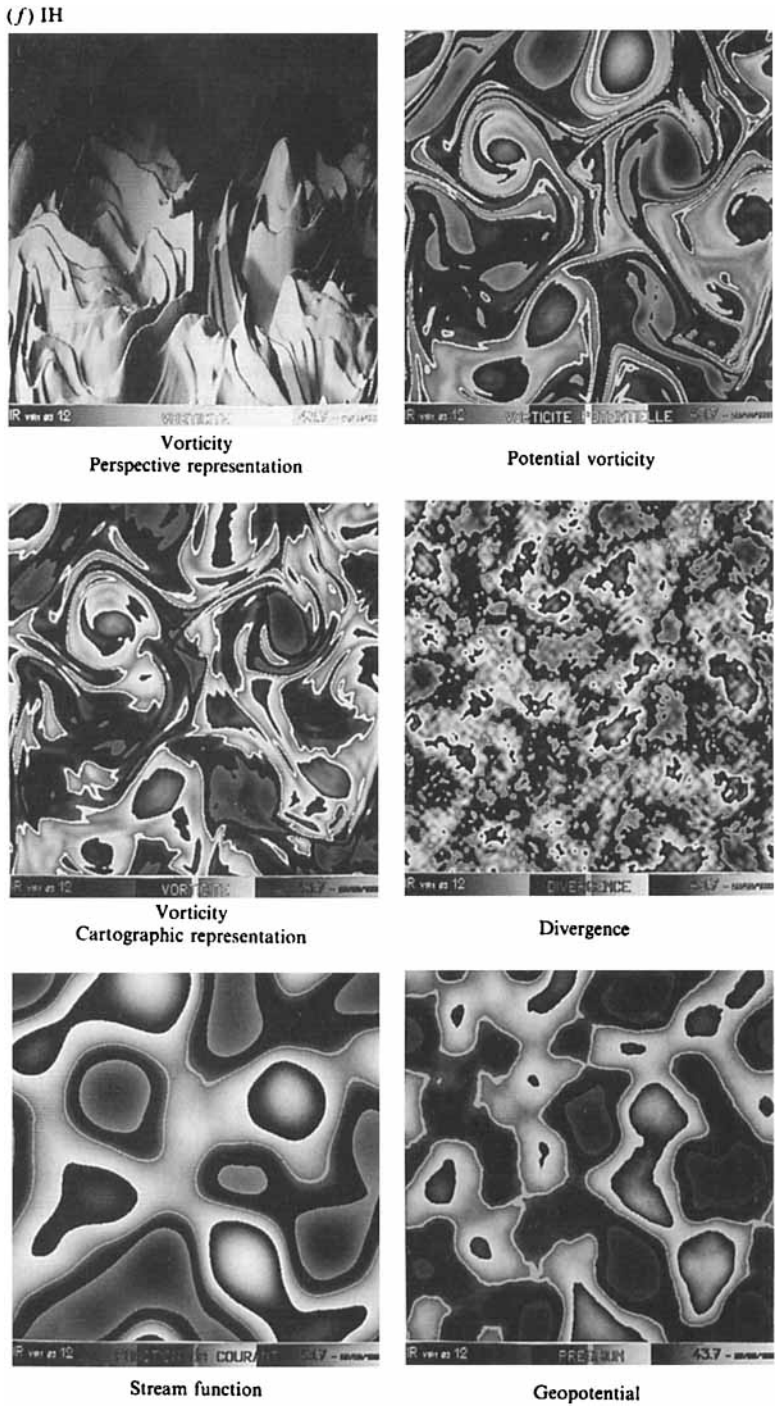

FIGURE 6. Spatial structure of five different fields (vorticity, potential vorticity, divergence, stream function and geopotential), describing the state of six different flows: (*a*) flow initially in balance equilibrium with moderate rotation, experiment BM at $t_{max} = 377$; (*b*) flow initially in balance equilibrium with high rotation, experiment BH at $t_{max} = 2262$; (*c*) flow initially mostly rotational with moderate rotation, experiment RM at $t_{max} = 377$; (*d*) flow initially mostly rotational with high rotation, experiment RH at $t_{max} = 2262$; (*e*) flow initially purely irrotational with moderate rotation, experiment IM at $t_{max} = 377$; (*f*) flow initially purely irrotational with high rotation, experiment IH at $t_{max} = 2262$.

spectra remain almost frozen, while the potentio–vortical spectra evolve slowly towards a slope close to k^{-4} (figure 3*b*,*d*,*f*). Little energy reaches the dissipation scales, which is consistent with the quasi-conservation of total energy already observed and discussed in §6.1 for high rotation rates. This inhibition of the nonlinear transfer among the inertio–gravitational modes is relatively straightforward on phenomenological grounds. An increase of the rotation rate increases the frequencies of inertio–gravity waves, which eventually get higher than the nonlinear frequencies in the spectral domain of the model. The group velocity increases, as well as frequency, and inhibition takes place because wave packets are able to disperse before any nonlinear interaction occurs. This type of behaviour has already been found in Rossby wave turbulence (Rhines 1975) and rotating three-dimensional turbulence (Roy 1986); in both cases the linear frequency ω_{L} is a non-decreasing function of wavenumber, while the nonlinear frequency ω_{NL} increases with it: hence the inhibition domain, characterized by $\omega_{\mathrm{NL}} < \omega_{\mathrm{L}}$, is restricted to the large scales. A similar argument applies here. The linear frequencies ω_{G} ($(1+k^2)^{\frac{1}{2}}$ in our non-dimensional notation) are an increasing function of wavenumber. On the other hand, in the absence of rotation (i.e. for $k > 1$), the k^0 spectrum we observe for the inertio–gravitational energy indicates nonlinear frequencies ω_{NL} increasing with wavenumber as $k^{\frac{3}{2}}$, therefore faster than ω_{G}. This implies that the inhibiting effect of rotation will be felt first in the larger scales.

At scales smaller than the Rossby deformation radius ($k > 1$), the distribution of inertio–gravitational energy is no longer frozen by rotation: its spectrum evolves towards a rather flat shape close to k^0 (figure 3*c*, *e*); this tendency is weaker but still noticeable in the initially balanced case (figure 3*a*). A similar behaviour has been observed by Herring *et al.* (1987), Métais & Herring (1989), for the internal wave spectrum in certain types of stratified flows. If we remember that the initial inertio–gravitational energy is always strongly peaked in the large scales ($k_I = 3$), a trend towards a flat spectrum indicates intense inertio–gravitational energy transfer towards smaller scales. This transfer is consistent with the energy dissipation already mentioned in §6.1 for turbulence affected by inertio–gravitational modes and slowly rotating (figure 2*c*, *e*).

This tendency towards a k^0 spectrum disagrees with the $k^{-\frac{5}{3}}$ spectral law that we have predicted for inertio–gravity waves on phenomenological grounds (Farge 1988) and with the $k^{-\frac{11}{7}}$ spectral law proposed by Zakharov & Sagdeev (1970) for non-dispersive two-dimensional acoustic turbulence, whose physics is similar to the non-rotating shallow-water dynamics. It cannot be explained by a lack of dissipation for the inertio–gravitational energy, because if we add an Asselin filter (Asselin 1972) to selectively damp the inertio–gravity waves, the same k^0 tendency remains for the scales intermediate between the injection k_I and the dissipation k_D wavenumbers (figure 7). It is important to notice that the potentio–vortical energy spectrum stays unchanged whatever damping is used for the inertio–gravitational energy, which confirms the lack of transfer between the potentio–vortical and the inertio–gravitational modes already mentioned in §6.1.

The observed k^0 spectrum, steeper than an equipartition spectrum, which would be k^{+1}, is related to the shape of the shocks which would develop in absence of dissipation. Indeed, the shallow-water model, contrary to the Korteweg–de Vries model, is not dispersive and therefore produces shocks due to wave breaking. This wave breaking, which would be possible in the absence of dissipation, is easy to understand if we consider the simple case of a wave propagating with amplitude h' in a shallow fluid layer of mean depth H. The ridge and the trough of the wave travel

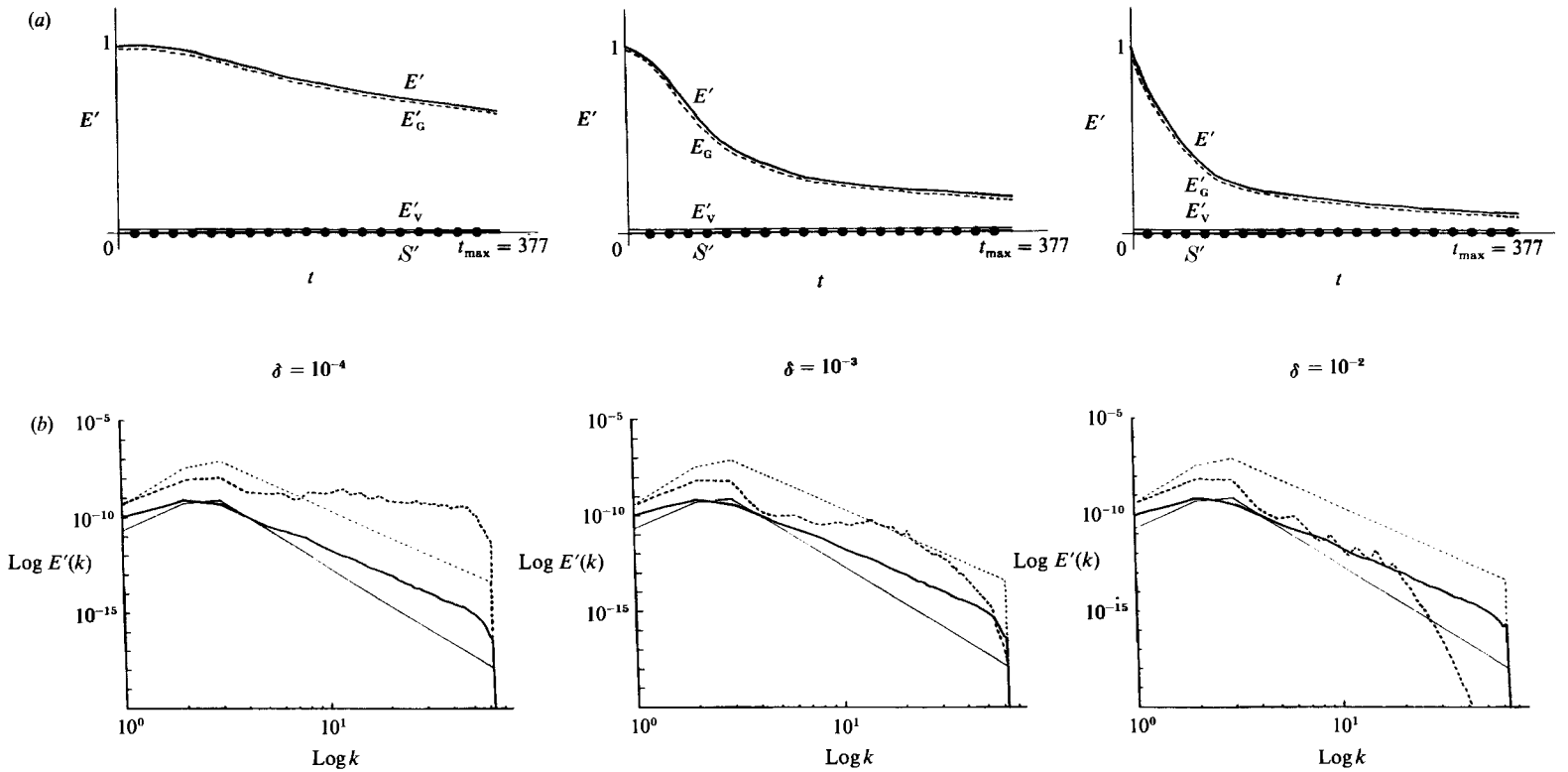

FIGURE 7. Experiment IM with three different dampings δ of the inertio–gravity waves using an Asselin filter: (*a*) time evolution, from $t = 0$ to $t = t_{max}$, of potential enstrophy S' (—●—●—●—), total energy E' (———), potentio–vortical energy E'_V (———) and inertio–gravitational energy E'_G (– – –); (*b*) unidimensional spectra, at $t = 0$ (thin lines) and $t = t_{max}$ (thick lines), of potentio–vortical energy (———) and inertio–gravitational energy (– – –).

respectively with velocities $(g(H+h'))^{\frac{1}{2}}$ and $(g(H-h'))^{\frac{1}{2}}$; therefore the ridge moves faster than the trough and the wave must eventually break. In fact such behaviour is not realistic, because in an actual fluid the shocks will get dispersed (as for the Korteweg de Vries model) through the emission of capillary ripples, which then will limit the process of wave breaking. But in the shallow-water model the dissipation may play the same role as dispersion in damping the strong geopotential gradients before shocks get formed and eventually break. It is important to notice that we are still in the domain of validity of the shallow-water hypothesis, because the smallest spatial scales considered here remain ten times larger than the water depth, and the vertical velocities are negligible, although their gradients may be strong.

6.5. *Inertio–gravity waves*

In studying and comparing the morphology of some of the fields viewed in physical space, we can visualize the structure of inertio–gravity waves. The difference between the geopotential and the stream-function fields corresponds to the potential part of the inertio–gravity waves. Likewise, the difference between the vorticity and the potential vorticity fields gives us information on the structure of the kinetic part of inertial waves, because they are actually rotational but have no potential vorticity. The divergence field readily shows us the structure of the kinetic part of gravity waves. We observe that, for all the cases where inertio–gravity waves are initially dominant (figure 6*d*, *e*, *f*), they eventually become strongly excited at small scales when rotation is small (figure 6*e*); this is consistent with the development of the direct inertio–gravitational energy cascade already noted in §6.1. On the other hand, inertio–gravity waves remain trapped in the larger scales when rotation is high (figure 6*d*, *f*), owing to the inhibition of their nonlinear cascade by rotation, also discussed in §§6.1 and 6.4.

6.6. *Geostrophic adjustment*

The geostrophic adjustment mechanism is indeed the capacity of shallow-water dynamics to transfer to smaller scales, and eventually dissipate, its inertio–gravitational energy (Sadourny 1975). We conclude from our experiments that an increase of the rotation rate inhibits this geostrophic adjustment process; in all cases, the proportion of inertio–gravitational energy to potentio–vortical energy in the larger scales increases with rotation (Farge & Sadourny 1986*b*). This seems, at first sight, a paradox, because one intuitively thinks that an increase of the external rotation should enhance the rotational part of the flow and therefore facilitate the adjustment process. This is indeed not the case because rotation inhibits all nonlinear transfers and therefore confines the inertio–gravity waves to the scales larger than the Rossby deformation radius (see §6.4).

A very straightforward parallel can be drawn with the effect of rotation on three-dimensional turbulence, as demonstrated in the laboratory by Wigeland & Nagib (1978), later simulated on a computer by Bardina, Ferziger & Rogallo (1985) and then by Roy (1986): three-dimensional turbulence does not become two-dimensional when rotation is applied, because the inhibition of transfers due to the waves keeps the three-dimensional spectral distribution of energy in its initial configuration. A similar process is occurring here: if inertio–gravitational energy is initially present in the larger scales, the inhibition of transfers due to rotation will confine it there.

Note that geostrophic balance in the small scales is never obtained in our experiments, except when we start from balanced initial conditions. This is readily

seen on the energy spectra of figure 3(*c–f*), and can also be recognized if we compare the geopotential and stream-function charts on figure 6(*c–f*).

6.7. *The reverse energy cascade*

The reverse energy cascade which may affect the potentio–vortical energy is the last aspect to be considered here. It can be looked upon in terms of energy spectra, but the discussion is perhaps easier if we study the stream-function charts in physical space (figure 6): the efficiency of the reverse potentio–vortical energy cascade process is measured by an increase of the dominant scale in the stream-function field during the flow evolution.

The strongest reverse potentio–vortical energy cascade occurs at low rotation rates and low inertio–gravitational energy levels (figure 2*a*, *c*), which corresponds to the cases where the process generating coherent vortices is most efficient (see §6.3). This perhaps sustains an argument given by Babiano *et al.* (1987), which links coherent vortex formation to local reverse energy cascade.

In all other cases, the reverse potentio–vortical energy cascade appears weakened, either by fast rotation, or by an excess of inertio–gravitational energy at large scales (figure 2*d–f*), which then departs from classical two-dimensional dynamics. For quasi-geostrophic flows (see §3), i.e. in the absence of inertio–gravity waves, we recall equation (19), approximately $S''(k) = (1+k^2)E''(k)$, which relates potential enstrophy S'' to quasi-geostrophic energy E''. In the limit of slow rotation ($k \gg 1$), (19) reduces to $S''(k) = k^2E''(k)$, which leads to a reverse energy cascade, by imposing that only potential enstrophy cascades towards small scales. On the contrary, for quasi-geostrophic flows subject to fast rotation ($k \ll 1$), (19) yields $S''(k) = E''(k)$; in that case, potential enstrophy disappears as a separate invariant and the reverse energy cascade is inhibited (Holloway 1983), the flow dynamics being then governed by a single invariant as for three-dimensional flow.

7. Conclusion

The purpose of this work was to investigate how two-dimensional turbulence is modified when the incompressibility constraint is removed. Therefore we have studied the interaction between inertio–gravitational and potentio–vortical modes within the framework of the Saint-Venant (shallow-water) equations. The first conclusion concerns the presence of isolated coherent vortices emerging out of the flow. They are formed when the level of inertio–gravity waves remains weak, and when rotation is small enough not to inhibit the direct potential enstrophy cascade, which then isolates vortices from each other by a background flow dominated by vorticity filaments passively advected by the mean flow. We have found that the smallest scales are concentrated inside the vortex cores and not on their periphery; this observation seems general to all two-dimensional flows.

In the range of parameters we have explored, we have not found interactions in the sense of energy exchanges between the two types of modes. At small scales, the two components of the motion appear to a large extent decorrelated: the potentio–vortical component behaves as if the flow were incompressible; on the other hand, we observe a cascade of inertio–gravitational energy towards small scales, as expected from the theory of statistical equilibria. In the larger scales, however, the presence of inertio–gravitational energy tends to inhibit the reverse cascade of potentio–vortical energy. Thus, even though there is no energy exchange between

the two components of the motion, one may influence the internal redistribution of modal energy within the other.

An interesting aspect of the dynamics of Saint-Venant equations compared to classical two-dimensional turbulence is that the removal of the incompressibility constraint makes the flow sensitive to the presence of rotation. We have shown that fast rotation tends to inhibit the transfers of potential enstrophy towards small scales, as well as the transfers of potentio–vortical energy towards larger scales. Further, rotation also reduces the direct inertio–gravitational energy cascade within the range of scales larger than the Rossby deformation radius; this has the important consequence that fast rotation inhibits the geostrophic adjustment process in the larger scales inasmuch as inertio–gravitational energy remains trapped there.

We thank a referee for correcting an error in §3 and suggesting several improvements of the paper. We also thank Ted Shepherd for his stimulating comments. The computing has been run on the Cray-1 and Cray-2 of C_2VR, Palaiseau, using as front-end the IBM-3090 of CIRCE, Orsay. We calculated the wavelet transform on a Sun-3 using a code developed by Ginette Saracco and adapted by Gabriel Rabreau. High-resolution raster displays have been done at LACTAMME, Ecole Polytechnique, on a prototype system designed by Jean-François Colonna. The manuscript has been typed by M. C. Roos-Cally.

REFERENCES

Asselin, R. 1972 Frequency filter for time integrations. *Mon. Weather Rev.* **100**, 487–490.

Babiano, A., Basdevant, C., Legras, B. & Sadourny, R. 1984 Dynamiques comparées du tourbillon et d'un scalaire passif en turbulence bidimensionnelle incompressible. *C.R. Acad. Sci. Paris* **299** II, 601–604.

Babiano, A., Basdevant, C., Legras, B. & Sadourny, R. 1987 Vorticity and passive scalar dynamics in two-dimensional turbulence. *J. Fluid Mech.* **183**, 379–397.

Bardina, J., Ferziger, J. H. & Rogallo, R. S. 1985 Effect of rotation on isotropic turbulence: computation and modelling. *J. Fluid Mech.* **154**, 321–336.

Basdevant, C., Legras, B., Sadourny, R. & Beland, M. 1981 A study of barotropic model flows: intermittency, waves and predictability. *J. Atmos. Sci.* **38**, 2305–2326.

Basdevant, C. & Sadourny, R. 1975 Ergodic properties of inviscid truncated models of two-dimensional incompressible flows. *J. Fluid Mech.* **69**, 673–688.

Batchelor, G. K. 1969 Computation of the energy spectrum in homogeneous two-dimensional turbulence. *Phys. Fluids* Suppl. II, **12**, 233–239.

Bennett, A. F. & Haidvogel, D. B. 1983 Low-resolution numerical simulation of decaying two-dimensional turbulence. *J. Atmos. Sci.* **40**, 738–748.

Boer, G. J. & Shepherd, T. G. 1983 Large-scale two-dimensional turbulence in the atmosphere. *J. Atmos. Sci.* **40**, 164–184.

Cahn, A. 1945 An investigation of the free oscillation of a simple current system. *J. Met.* **2**, 113–119.

Charney, J. 1971 Geostrophic turbulence. *J. Atmos. Sci.* **28**, 1087–1095.

Couder, Y. 1984 Two-dimensional grid turbulence in a thin liquid film. *J. Phys. Lett.* **45**, 353–360.

Craya, A. 1958 Contribution à l'analyse de la turbulence associée à des vitesses moyennes. *P.S.T. Ministère de l'Air*, p. 345.

Desbois, M. 1975 Large-scale kinetic energy spectra from Eulerian analysis of Eole wind data. *J. Atmos. Sci.* **32**, 1838–1847.

Dritschel, D. G. 1986 The nonlinear evolution of rotating configurations of uniform vorticity. *J. Fluid Mech.* **172**, 157–182.

ERRICO, R. M. 1981 An analysis of interactions between geostrophic and ageostrophic modes in a simple model. *J. Atmos. Sci.* **38**, 544–553.

ERRICO, R. M. 1984 The statistical equilibria solution of a primitive equations model. *Tellus* **36A**, 42–51.

FARGE, M. 1987 Normalization of high-resolution raster display applied to turbulent fields. In *Advances in Turbulence* (ed. G. Comte-Bellot), pp. 111–123. Springer.

FARGE, M. 1988 Nonlinear dynamics of inertio–gravity waves. In *59th Varenna Course on Nonlinear Topics in Ocean Physics* (ed. A. Osborne). North-Holland.

FARGE, M. & LACARRA, J. F. 1988 The numerical modelling of shallow water equations. *J. Méc. Théor. Appl., Special Issue, Suppl.* 2 to **7**, 63–86.

FARGE, M. & RABREAU, G. 1988 Wavelet transform to detect and analyse coherent structures in two-dimensional turbulent flows. *C.R. Acad. Sci. Paris* **307** II, 1479–1486.

FARGE, M. & SADOURNY, R. 1986*a* Inhibition de la turbulence bi-dimensionnelle par une rotation d'entraînement. *C.R. Acad. Sci. Paris* **302** II, 847–850.

FARGE, M. & SADOURNY, R. 1986*b* Effets des ondes d'inertie–gravité sur une turbulence bi-dimensionnelle non forcée en rotation. *C.R. Acad. Sci. Paris* **303** II, 881–886.

FEIEREISEN, W. J., REYNOLDS, W. C. & FERZIGER, J. H. 1981 Numerical simulation of a compressible homogeneous turbulent shear flow. *Mechanical Engineering Department, Rep.* TF-13. Stanford University.

FORNBERG, B. 1977 A numerical study of two-dimensional turbulence. *J. Comput. Phys.* **25**, 1–31.

FOX, D. G. & ORSZAG, S. H. 1973 Inviscid dynamics of two-dimensional turbulence. *Phys. Fluids* **16**, 167–171.

HERRING, J. R. 1974 Approach of axisymmetric turbulence to isotropy. *Phys. Fluids* **17**, 859–872.

HERRING, J. R. & MCWILLIAMS, J. C. 1985 Comparison of direct numerical simulation of two-dimensional turbulence with two-point closure: the effects of intermittency. *J. Fluid Mech.* **153**, 229–242.

HERRING, J. R., MCWILLIAMS, J. C., MÉTAIS, O. & GAMAGE, N. 1987 Vortical turbulence in a stratified fluid. *Third Int. Symp. on Stratified Flows, IAHR meeting, Pasadena, February 3–5.* Preprints.

HOLLOWAY, G. 1983 Effects of planetary wave propagation and finite depth on the predictability of atmospheres. *J. Atmos. Sci.* **40**, 314–327.

HOPFINGER, E. J. 1983 The structure of turbulence in homogeneous and stratified rotating fluids. *J. Méc. Special Issue on Two-Dimensional Turbulence*, pp. 21–44.

HOYER, J. M. & SADOURNY, R. 1982 Inhibition of baroclinic instability of low-resolution models. *J. Atmos. Sci.* **39**, 2138–2143.

KRAICHNAN, R. H. 1967 Inertial ranges of two-dimensional turbulence. *Phys. Fluids* **10**, 1417–1423.

LEITH, C. E. 1968 Diffusion approximation for two-dimensional turbulence. *Phys. Fluids* **11**, 617–673.

LEITH, C. E. 1980 Nonlinear normal mode initialization and quasi-geostrophic theory. *J. Atmos. Sci.* **37**, 958–968.

LILLY, D. K. 1983 Stratified turbulence and mesoscale variability of the atmosphere. *J. Atmos. Sci.* **40**, 749–761.

LORENZ, E. N. 1980 Attractor sets and quasi-geostrophic equilibrium. *J. Atmos. Sci.* **37**, 1685–1699.

LORENZ, E. N. 1986 On the existence of a slow manifold. *J. Atmos. Sci.* **43**, 1547–1557.

MCWILLIAMS, J. 1984 The emergence of isolated coherent vortices in turbulent flow. *J. Fluid Mech.* **146**, 21–43.

MÉTAIS, O. & HERRING, J. R. 1989 Numerical experiments in forced stably stratified turbulence. *J. Fluid Mech.* **202**, 97–115.

MOREL, P. & LARCHEVÊQUE, M. 1974 Relative dispersion of constant-level balloons in the 200-mb general circulation. *J. Atmos. Sci.* **31**, 2189–2196.

MOYAL, J. E. 1952 The spectra of turbulence in a compressible fluid eddy turbulence and random noise. *Proc. Camb. Phil. Soc.* **48**, 329.

MÜLLER, P., LIEN, R. C. & WILLIAMS, R. 1988 Estimate of potential vorticity at small scales in the ocean. *J. Phys. Oceanogr.* **18**, 401–416.

OBUKHOV, A. 1949 On the question of geostrophic winds. *Izv. Akad. Nauk. SSSR, Geogra. Geofiz.* **13**, 281–306.

RIABOUCHINSKY, D. 1932 Sur l'analogie hydraulique des mouvements d'un fluide compressible. *C.R. Acad. Sci. Paris* **195**, 998.

RHINES, P. B. 1975 Waves and turbulence on a beta-plane. *J. Fluid Mech.* **69**, 417–443.

RHINES, P. B. 1979 Geostrophic turbulence. *Ann. Rev. Fluid Mech.* **11**, 401–441.

RILEY, J. J., METCALFE, R. W. & WEISSMAN, M. A. 1981 Direct numerical simulations of homogeneous turbulence in density-stratified fluids. *Proc. AIP Conf. on Nonlinear Properties of Internal Waves*, pp. 79–112.

ROY, P. 1986 Simulation numérique d'un champ turbulent homogène incompressible soumis à des gradients de vitesse moyenne. Thèse d'état, Université de Nice.

SADOURNY, R. 1975 The dynamics of finite-difference models of the shallow-water equations. *J. Atmos. Sci.* **32**, 680–689.

SADOURNY, R. 1985 Quasigeostrophic turbulence. In *88th Varenna Course on Turbulence and Predictability in Geophysical Fluid Dynamics and Climate Dynamics* (ed. M. Ghil). North-Holland.

SADOURNY, R. & BASDEVANT, C. 1985 Parametrization of sub-grid scale barotropic and baroclinic eddies in quasi-geostrophic models: the anticipated potential vorticity method. *J. Atmos. Sci.* **42**, 1353–1363.

SAFFMAN, P. G. 1971 On the spectrum and decay of random two-dimensional vorticity distributions at large Reynolds number. *Stud. Appl. Maths* **50**, 377–383.

SALMON, R. 1978 Two-layer quasi-geostrophic turbulence in a simple special case. *Geophys. Astrophys. Fluid Dyn.* **10**, 25–51.

SOMMERIA, J. 1986 Experimental study of the two-dimensional inverse energy cascade in a square box. *J. Fluid Mech.* **170**, 139–168.

TEMPERTON, C. 1983 Very fast real Fourier transforms. In *Special Topics and Applied Mathematics*, pp. 165–171. North-Holland.

WARN, T. 1986 Statistical mechanical equilibria of the shallow-water equations. *Tellus* **38A**, 1–11.

WIGELAND, R. A. & NAGIB, H. M. 1978 Grid-generated turbulence with and without rotation about the streamwise direction. *11th Fluid and Heat Transfer Rep.* R.78-1. Illinois Institute of Technology.

ZABUSKY, N. J. 1984 Contour dynamics: a method for inviscid and nearly inviscid two-dimensional flows. *Proc. IUTAM Symp. on Turbulence and Chaotic Phenomena* (ed. T. Tatsumi), pp. 251–257. North-Holland.

ZAKHAROV, V. E. & SAGDEEV, R. Z. 1970 Spectrum of acoustic turbulence. *Sov. Phys. Dokl.* **15**, 439–441.